UNIVERSIDADE DA BEIRA INTERIOR
Engenharia

Solar System for a Long Endurance Electric UAV

Joana Carlota Caires Sousa

Dissertação para obtenção do Grau de Mestre em
Engenharia Aeronáutica
(Ciclo de estudos integrado)

Orientador: Professor Doutor Pedro Vieira Gamboa

Covilhã, outubro de 2015

Acknowledgments

I would like to thank my supervisor Doctor Pedro Gamboa for his technical guidance and knowledge of aircraft design. A special acknowledgement to Pedro Santos and Pedro Alves for their friendship and support throughtout my dissertation work.

Mário, for his endless patience.

Dad, you were there whenever I needed someone to talk, and you have been a great father and friend to me. Finally, to my mother for having supported me during all these years, for her patience, kindness and love.

Resumo

Os combustíveis fosséis, carvão, petroléo e gás natural, constituem a maior parte das fontes de energia primária a nível mundial. Sendo a energia essencial ao bem-estar da população e ao desenvolvimento da sociedade, produzir e utilizar energia de forma sustentável é vital para a humanidade. Porém, a dependência de combustíveis fosséis é demasiado elevada e sendo esta uma fonte limitada na natureza, é necessário contrariar o seu uso nos diversos setores. Na Indústria Aeroespacial a utilização de painéis solares é uma alternativa executável.

Esta Dissertação de Mestrado inclui um plano concetual de um sistema propulsivo elétrico, destinado a um UAV com uma envergadura de 4,5 m e um peso de aproximadamente 52 N. A construção deste sistema é particularmente diferente dos métodos convencionais de propulsão, pelo que o seu projeto e dimensionamento dependem especialmente da energia disponível armazenada na bateria, e da potência gerada pelos painéis solares.

Devido à variação da intensidade de radiação solar em diferentes zonas do país e do ano, foi elaborado um plano de testes experimentais para verificar a viabilidade do sistema. Estes testes demonstram que a potência disponível é especialmente influenciada pelo eixos vertical e longitudinal, dados por arfagem e pranchamento. Embora seja uma aeronave de pequenas dimensões, a asa para além da sua função aerodinâmica, possui uma zona adequada aquando a colocação das células solares, deste modo, recorrendo uma diferenciação de segunda ordem é demonstrado que esta colocação seria ideal a 1,5 cm do bordo de fuga.

Ainda, uma simulação da missão foi realizada no Túnel de Vento da Universidade da Beira Interior atingindo o seu propósito com sucesso. Portanto, é estudado o posicionamento apropriado dos módulos solares, desenvolvido um método de fixação à Estrutura Alar e projetado o circuito elétrico de modo a realizar um voo sustentável.

Palavras-chave

UAV, Indústria Aeroespacial, Propulsão elétrica, Radiação Solar, Voo Sustentável

Abstract

Fossil fuels such as coal, oil and natural gas, are the worldwide primary energy resources. Energy is essencial to the peoples' well-being and society development, as it is known today and expected in the future to produce and use energy in a sustainable way is vital to our civilization. However, dependence on fossil fuel is awfully high and it is necessary to hinder their use in several industries as it is a limited resource. In the Aeroespace Industry solar energy has been gaining widespread development, becoming the solution to many negative factors.

This Master Thesis includes a conceptual design of an electric propulsion system for a UAV with a wingspan of 4.5 m and a weight of approximately 52 N. The construction of this system is different from conventional propulsion methods, so the design and sizing rely on the available energy stored in the battery and the power generated by the solar panels. As solar radiation is different throughout the year, a plan for experimental tests was drafted to verify the system viability. Experiments show that exact azimuth orientation is not critical, vertical axis given by pitch and roll, have a more important effect on performance. Although it is a small aircraft, the wing beyond its aerodynamics function, has a proper zone where solar cells should be placed. Appealing to a second order differentiation it is possible to determine that solar panels should be placed at 1.5 cm from the trailing edge affecting as little as possible the airfoil.

A mission simulation was done to understand the propulsion system feasibility. Although, the eight hour sustainable-flight was not possible to replicate the motor still ran for 5 hours, being the battery charged during cruise phase as pretended. Therefore, proper solar cells placement, development of a mounting method and electrical circuit design are carried out in order to allow the UAV to achieve a sustainable-flight.

Keywords

UAV, Aeroespace Industry, Electric propulsion, Solar Radiation, Sustainable-Flight.

Contents

List of Figures

List of Tables

Glossary

CPV	Concentrating PV
CZ	Czochralski
DOD	Departament of Defense
ERAST	Environmental Research Aircraft Sensor Technology
Group III	Chemical elements of group 13 of the periodic table
Group V	Chemical elements of group 15 of the periodic table
JST	Japan Solderless Terminal
MJ	Multijunction
MPPT	Maximum Power Point Tracker
NREL	National Renewable Energy Laboratory
OPV	Organic PV
PV	Photovoltaic
STC	Standard Test Conditions
UAV	Unmanned Aerial Vehicle

Nomenclature

A	Solar cell area
$a-Si$	Amourphous Silicon
$a-Si:H$	Hydrogenated amourphous Silicon
b	Wingspan
c	Wing mean chord
$CdTe$	Cadium Telluride
$CIGS$	Cooper indium gallium selenide
$C-si$	Crystalline Silicon
d	Travelled distance
D_{stage}	Aircraft drag
$Imax$	Maximum Solar Irradiance
I_{MPP}	Nominal power Current
I_{SC}	Short-Circuit Current
E_{req}	Propulsive energy required
g	Gravitational constant
η_B	Battery efficiency
η_C	Cables efficiency
η_{ESC}	Electronic speed controller efficiency
η_{Pstage}	Propeller efficiency
η_{Mstage}	Electric motor efficiency
η_{stage}	Total componentes efficiency
ηPV	Solar cell efficiency
P	Power
p	Perimeter of a circular turn
$Pmax$	Solar cell maximum power ouput
P_{MPP}	Nominal Power
P_{req}	Propulsive required power
R_{sh}	Shunt resistance
$Sref$	Wing area
t	Duration of a full lap loiter pattern

t_{stage}	Duration of each stage
$\mu c - Si:H$	Microcrystalline Silicon
v	Aircraft average cruise speed
V_{MPP}	Nominal power Voltage
V_{OC}	Open-Circuit voltage
v_{stage}	Each stage aircraft speed
W	Take-off weight
φ	Pitch angle

Chapter 1

Introduction

1.1 Motivation

Solar Energy is very important in various industries since it is a clean energy extracted by Solar Radiation. In the Aerospace industry, this is the key to many negative factors such as environmental pollution, noise and the dependence of fuel witch is a limited resource in nature.

The main motivation comes from the environmental challenges that the planet is going through. Since global warming until the lack of natural resources. The commercial aircraft today use a large amount of fuel which has a negative impact on the atmosphere due to release of carbon. One way to solve this problem would be to eliminate fossil fuels and finding an alternative, as hydrogen or biofuels, however that may also be depleted over time. Thus, a propulsion system using solar energy not only can be successful, as may also be the future and the solution to all the environmental problems in aviation.

1.2 Objectives

Initially it is necessary to select the type of mission and the energy requirements that are needed. Once the mission is chosen it follows the design propulsion system with all the details to achieve a sucessful mission. So the leading goal is to project a propulsion system that provide a sustainable-flight.The requirements include:

1. Definition of the propulsion system architecture;
2. Size photovoltaic cells and solar arrays;
3. Desgin an attachament system for the solar panels;
4. Design and assemble the electronic circuit.
5. Develop a solar panel experiments guideline;
6. Assemble the system.

1.3 Structure of the Document

This master thesis first starts with a theoretical background related to the main work done, where a brief history of solar-powered aircraft is discussed as well as other UAV studies.It then continues with the specification of the mission and the necessary energy requirements

to provide a sustainable-flight. Once the mission and the energy requirements are selected it follows the Propulsion System Architecture, in which, each different component of the solar powered system is described. On a following stage, it is studied the appropriate position of the solar cells on the wing and a found a method to mount them.

As it is expected, solar radition is different throughout the year, for this reason some experimental tests are conducted and reported. The results from the experiments are then compared with solar cells values concebed in a laboratory environment. This chapter enable to determine the solar cells efficiency and validate the propulsion system.

To finish, the conclusions will be stated at the end of this document as well as some considerations about future work.

Chapter 2

State-of-art

The achievement of a solar powered aircraft capable of continuous flight was still a dream some years ago, but this great challenge has become feasible today. In fact, significant progresses have been realized recently in the domains of flexible solar cells and high energy density batteries. In this section, a brief history of solar-powered aircraft will be discused, as well as other UAV studies that have been done over the last 40 years.To understand the history of solar- powered flight, a discussion of solar cells is also required.

2.1 Unmanned Aerial Vehicle

According to the Department of Defense of the United States of America[1] an unmanned aerial vehicle is defined "as powered, aerial vehicles that do not carry a human operator, use aerodynamic forces to provide vehicle lift, can fly autonomously or be piloted remotely, can be expendable or recoverable, and can carry a lethal or nonlethal payload. Ballistic or semi-ballistic vehicles, cruise missiles, and artillery projectiles are not considered UAV by the DOD definition. UAVs are either described as a single air vehicle (with associated surveillance sensors), or a UAV system, which usually consists of three to six air vehicles, a ground control station, and support equipment."

2.2 Solar Energy

The most plenteous energy resource that exists in the world is Solar Energy. Surely, the fee at which solar energy interceps the Earth is about 10,000 [2] times greater than the speed at which the humankind uses energy. Although not all countries are equally gifted with solar energy, it is possible for nearly all, a meaningful contribution from a combination of energy from direct solar radiation. The conversion of solar energy is a large family of different technologies to please a range of needs for energy services. Solar technologies can provide heating, cooling, natural lighting and electricity for a variety of applications.

2.2.1 The Photovoltaic Effect

On 1839 a french physicist first observed the physical phenomenon responsible for converting light to electricity, his name was Edmund Becquerel. He noted that a voltage acted when one of two indentical electrodes in a weak conducting solution was

illuminanetd. The PV effect was primarily studied in solids, such as selenium [(1)]. Selenium is capable to convert light in the visible part of the sun's spectrum and for then quickly adopeted by the then-emerging field of light- measuring devices. Selenium cells cost is too high relative to the insignificant amount of power they produce so they have never become pratical as energy converters. Meanwhile, work on the physics of PV effect has expanded and a main step forward in solar-cell technology took place on 1940 when the CZ *(for more information go to Annex* Appendix A) technique was developed for producing highly pure crystalline silicon.

According to "*Basic Photovoltaic Principles and Methods*" [3], "the Photovoltaic effect is the basic of conversion of light to electricity in photovoltaic or solar cells. Described simply, the PV effect is as follows: Light, which is pure energy enters a PV cell and imparts enough energy to some electrons (negatively charged atomic particles) to free them. A built-in-potencial barrier in the cell acts on these electrons to produce a voltage (the so-called photovoltage), which can be used to drive a current through a circuit" as can be seen on Figure 2.1.

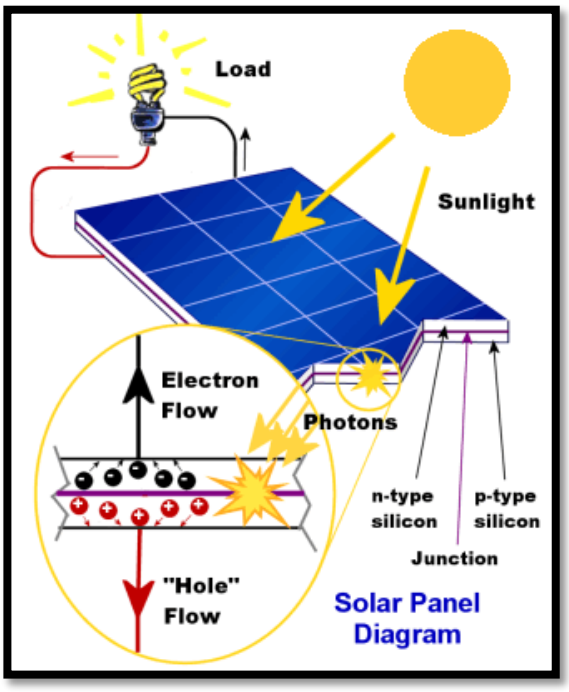

Figure 2.1- Photovoltaic Solar Panel Working Principle [4].

[(1)] **Selenium** – a nonmetallic element chemically resembling sulfur and tellurium, occurring in several allotropic forms, as crystalline and amorphous, and having an electrical resistance that varies under the influence of light. Symbol: Se; atomic weight: 78.96; atomic number: 34.

Charge carriers like electrons and holes are generated when sulingh raids a solar cell. The holes are drawn into the positive, p-layer, and the electrons are drawn into the negative,n-layer, both are separated by the internal fild produced by junction. When a circuit is made, the free electrons have to get through the load to recombine with the positive holes, thus producing current from the cells under illumination.

2.2.3 Photovoltaics Industry

The PV industry is rising, with rates of 30 % [5] per year over the last decade. This progresss has been determined by the market development programs to accelerate the deployment of sustainable energy options and rapidly increasing fossil fuel prices.This proves, if need be, that solar photovoltaics is on the way to becoming a major part of the eletricity system, delivering clean, safe and affordable energy to the greater number all around the globe.

2.2.3.1 Solar Cells Evolution

a) 1st Generation Solar Cells , Crystalline Silicon PV techonolgy (c-Si)

Silicon-based technology is the leading technology in the commercial production of solar cells, accounting for about 85% of the solar cell market. It is technically proven and has succeed in achieving market penetration, primarily in off-grid remote areas and lately in grid-connected applications. There are however, several limitations to this 1st generation technology from the onset. Silicon wafers are very fragile and the process involved in the manufacturing is difficult and labor intensive, therefore high cost. There are two types of crystalline, or wafer-based silicon PV: monocrystalline and multicrystalline. Monocrystalline semiconductor wafers are cut from single-crystal silicon ingots. Multicrystalline semiconductor wafers are cut from directionally solidified blocks or grown in thin sheets. Monocrystalline ingots are more difficult, energy intensive, and expensive to grow than simple blocks of multicrystalline silicon. However, monocrystalline silicon produces higher- efficiency cells.

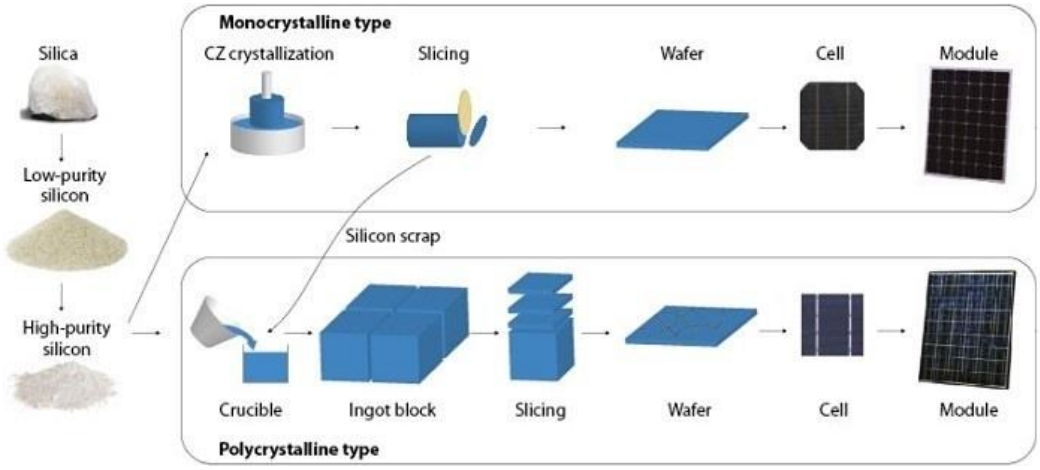

Figure 2.2- Production process for typical crystalline silicon solar cells [6].

The rated efficiencies of standard c-Si PV modules are about 14 % to 16 % for commercial scale and module efficiencies of about 17 % to 21 % for a laboratory scale [7].

b) 2nd Generation solar cells : Thin-Film technology solar cells

In order to cut down the manufacturing costs, thin-film solar cells appear as alternatives. The technology earns from the low processing temperature. Thin-film PV cells consist of a semiconductor layer a few microns (μm) of thickness, which is about 100 times thinner than current $C-si$ cells. Most thin films are direct bandgap semiconductors, which means they are capable of absorving energy contained in sunlight with a much thinner layer than traditional $C-si$ PV. The most common thin-film semiconductor materials are $CdTe$, $a-Si$ and $CIGS$.

The main disadvantage of $a-Si$ solar cell is the degration of their performance under light exposure over time. Another notable concept of $a-Si$ solar cells is hydrogenated amorphous silicon $a-Si:H$combined with microcrystalline silicon $\mu c-Si:H$ forming the multi-junction thin-film silicon solar cell. The advantage of $\mu c-Si:H$ is that it absorbs light from the red and near infrared part of the spectrum, thus increasing the efficiency.The potential drawbacks of $CdTe$ and $CIGS$ solar cells are materials availability for long-term use and issues with toxicity ($CdTe$) and mass production has been proven to be difficult ($CIGS$). The efficiency of the second generation solar cells varies from 11% to 20 % for laboratory scale and 9 % to 12 % for commercial scale[7].

c) 3rd Generation solar cells

Research for improving solar cell performance by enhancing its efficiency has led to the development of the third generation solar cells. Dye-sensitized solar cells use dye molecules absorbed onto a nanostructured substrate and immersed in a liquid to absorb solar radiation and have demonstrated laboratory efficiencies as high as 11.1 %. OPV solar cells, established on polymers or small molecules with semiconductor properties, have demonstrated laboratory cell efficiencies above 8 %. Organic modules have the potential for low-cost manufacturing using existing printing and lamination technologies.

There are significant challenges to the commercialization of solution-processed organic solar cells and dye-sensitized, due to the stability of the materials against oxygen and water ingress. This limits the lifetime of these devices to anywhere from a few hundred hours to 2 years. This issue is being addressed through efforts to develop improved, yet cost-effective, encapsulants. In addition, organic and dye-sensitized solar cells use dyes that have been shown to degrade when put in direct sunlight for long periods of time, a significant issue to have in a solar cell[7].

d) Concentrating PV

CPV uses mirros or lenses made out of low-priced materials such as glass, steel, and plastic to focus sunlight onto a relatively small semiconductor area. This technique have several significant advantages. First, it reduces the amount of active semiconductor material needed to produce a given amount of electricity. On an area basis, the active semiconductor material is the most complex and expensive component of many PV modules; this is particularly true for MJ cells. MJ cells are capable of much higher efficiencies than single junction silicon or thin-film cells. This is because each junction of a MJ cell is designed to collect a different part of the solar spectrum: MJ cells are typically a load of three different cells on top of one another. This higher efficiency comes at an increase in manufacturing cost, and thus MJ devices are too expensive to use in terrestrial applications without concentration. The downside to CPV, especially for higher concentration levels, is that, in order to maintain the concentration of sunlight on the cell, the module must accurately follow the sun throughout the day. Tracing results in a more complex and expensive installation. Recent improvements to MJ PV cells have produced cell efficiencies of 43.5 % in the laboratory[7].

2.4 NREL's world wide best research in laboratory

The Chart shown on figure 1, summarizes the world wide research effort over the last 40 years. These solar cells are concebed in a laboratory environment and their area is not often larger than 1 square centimeter.

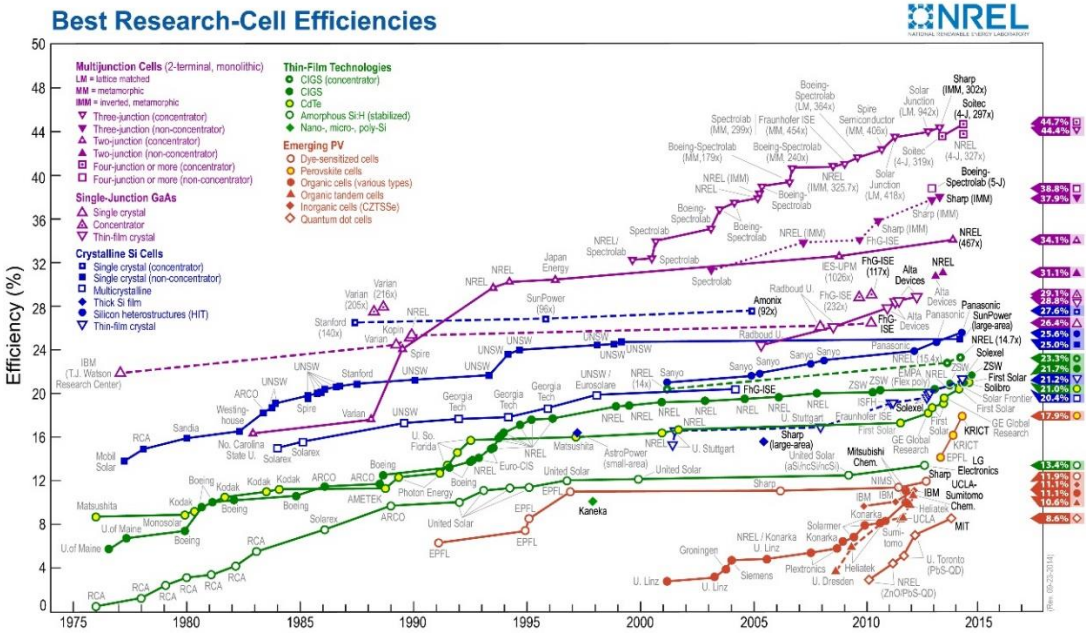

Figure 2.3- World Wide Best Research cell efficiencies over the last 40 years in laboratory [8].

The devices included in this plot have efficiencies that are confirmed by independent, recognized test laboratories and are reported on a standardized basis. The measurements for new entries must be according to standard test or reporting conditions (STC). As can be seen on Figure 2.2, cell efficiency results are provided with diferents families of semiconductors as well as some 26 different subcategories. These diferents familes of semiconductors are indicated by distinctive colored symbols. The purple colored, Multijunction and Single Gallium Arsenide cells markers, represents the III-V technology (a combination of group III and group V, called III-V semiconductors), based on single, double and triple junctions and have efficiencies ranging from 26 % up to 44 % under concentrated light conditions. The blue lines and dots represente the crystalline silicon technology based on monocrystalline and multicrystalline silicon which record efficiencies range from 20.4 % to 27.6 %. The inorganic thin-film techonologies, like thin-film silicon, $CdTe$ and $CIGS$ are indicated by the green markers and their record effiencies range from 13.4 % up to 20 %. The red colored lines and markers indicats the emerging PV techonologies like organic solar cells. It is necessary to take into account that these are laboratory results of a very small area of solar cells and this

chart does not tells us anything of the long term stability of some PV techonologies, certainly not the one indicated in red[9].

2.5 History of Unmanned Aerial Vehicles

The first aircraft flight powered by a solar propulsion system took place on the 4th of November 1974 at Camp Irwin in California. Sunrise I, flew 20 minutes at an altitude of 100 m throughout its inaugural flight. It had a wingspan of 9.76 m, weight of 12.25 kg and a power output of 450 W from 4096 solar cells .Regrettably, Sunrise I was seriously damaged when caught flying in a sand storm. An improved version, Sunrise II, was built and tested on the 12th of September 1975. With an equivalent wingspan, its weight was reduced to 10.21 kg and the 4480 solar cells were capable of delivering 600 W. After many weeks of testing, this second version was also damaged due to a failure in the command and control system. Despite all, the history of solar flight was engaged and its first demonstration was done[10].

Figure 2.4- Sunrise II, 1975 [11].

High Altitude Long Endurance Platforms and Eternal flight

The US government gave funding to AeroVironment Inc. to study the feasibility of long endurance solar electric flight above 19 000 km. As a result they patronized the **Pathfinder** project which accomplished it first flight at Dryden in 1993. When funding for this program ended, the 30 m wingspan and 254 kg aircraft became a part of NASA's ERAST program that started in 1994. In 1995, he exceeded Solar Challenger's altitude record for solar-powered aircraft when it reached 15 392 m and two years later he set the record to 21 802 m. In 1998, Pathfinder was modified into a new version, **Pathfinder Plus**, which had a bigger wingspan and new solar aerodynamic propulsion and system technologies. The main

objective was to validate these new elements before building its successor, the Centurion [10].

Figure 2.5- Pathfinder in Flight over Hawaii [12].

Figure 2.6- Pahtfinder- Plus in flight over Hawaii[13].

Centurion, which had a double wingspan compared to Pathfinder, was conceived to perform a flight powered by solar energy that coud stay airborne for weeks or months. Its goal was to achieve scientific sampling and imaging missions or serving as telecommunications relay platforms. It was capable to transport 45 kg of remote sensing and data collection instruments for use in scientific studies and also 270 kg of sensors, telecommunications and imaging equipment that could go up to 24 400 m of altitude.It would also have a lithium battery that could provide enough energy for two going up to five hours flight after sunset, but insufficient to fly whole night. [10]

Figure 2.7- Centurion, 1997-1999 [14].

Helios was the last prototype built. For NASA, the two main objectives were to demonstrate sustained flight at an altitude near 30 480 m and a continued flight for at least 24 hours, including 14 hours above 15240 m, at least. In 2001, Helios achieved the first goal near Hawaii with an unofficial world-record altitude of 29 524 m and a 40 minutes flight above 29 261 m. But unfortunately, it never reached the second objective as it was destroyed when it fell into the Pacific Ocean on June 26, 2003 due to structural failures[10].

Figure 2.8- Helios, 1999-2003 [15].

The Official World Record time for longest duration Unmanned Flight

Two Zephyr aircrafts were first trialed in New Mexico in December 2005 by a British company called QinetiQ, achieving a maximum duration of 6 hours and reaching an altitude of 7 925 m. After an 18 hours of flight in July 2006, one of the aicrafts developed by QinetiQ exceeded the official world record time for the longest duration unmanned flight with a 54 hour flight in New Mexico on the 10th of September 2007, reaching a maximum altitude of 17 786 m. Weighting only 30 kg for 18 m wingspan, the aircraft used solar power for the ascent, reverting to lithiumsulphur battery power as dusk fell. QinetiQ expects in the future flight duration of some months at an altitude above 15 240 m[16].

Figure 2.9- Zephyr 7, 2010 [17].

A Remarkable Project

One of the most remarkables projects of solar energy is Solar Impulse, which is a long range solar powered aircraft manned. It is headed by Bertrand Piccard, who co-piloted the first balloon to circle the world non-stop, and André Borschberg.

According to *Solar Impulse "The goal of the project is to fly around the world with zero fuel. This challenge will be undertaken by Solar Impulse's second generation aircraft, HB-SIB, which is currently under construction. It will be fully assembled in the spring of 2014 and will fly around the world a year later."*

The first Flight was executed on 2010 and at the same year they reached a long-duration flight of 26 hours, 10 minutes and 19 secondes. Solar Impulse in its inaugural flight accomplished three record: maximum altitude, endurance and gain height, 9235 m, 26h10m19s, 8744 m, respectively. The second Solar Impulse, HB-SIB construction started on 2011 and first flown on 2014. As André Borschberg said "It is the first aircraft which will have almost unlimited endurance." The wingspan would be 72 m, it would carry 17, 000 solar

cells that supply four electric motors and achieved an altitude of 5,500 m. The average ground speed was 56 km/h[18].

Figure 2.10 – Solar Impulse 2 in Abu Dhabi [19].

Chapter 3

Aircraft Description and Mission

This chapter first starts with the description of the aircraft mission and vehicle characterization, ending with a brief introduction to the non-conventional propulsion system powered by solar energy. The material presented here is part of a cooperative research project involving tree research units that belong to the line of Aeronautics and Space of LAETA [(2)], namely CCTAE [(3)], AEROG [(4)] and IDMEC [(5)].

3.1 Solar UAV Mission

The LEEUAV project aims to develop a Long Endurance Electric Unammaned Aerial Vehicle powered by solar energy that must be as light as possible and be able to carry a payload of 1 kg. UAVs are slighty more cost effective to acquire and operate than conventional manned aircraft, so the objective of this project is to create a reasonable cost platform that can be handly installed in areas with small space. The aircraft has to be able to collect and store energy for long endurance flight. The mission profile may be summarized as follows:

1. Take-off in a very short distance (in 8 m) or Launched by hand (in 3 m);
2. Climb to 1000 m above ground level for a cruise altitude, in 10 minutes;
3. Sustainable-flight of 8 hours at equinox with a flight cruise speed of no less than 7 m/s;
4. Descend from cruise altitude during 29 minutes to ground level without power;
5. Landing in the field.

The energy requirements have been calculate based on the efficiency of each component of the propulsion system in every stage of the mission. The efficiencies of battery, cables and electronic speed controlller ESC, are fixed for the entire mission while the efficiencies of the electric motor and propeller are different in each stage.The propulsive power required for each stage of the mission can be estimated as:

$$P_{req} = v_{stage} \times D_{stage} \tag{3.1}$$

[(2)] LAETA. Associated Laboratory for Energy, Transports and Aeronautics. Portugal

[(3)] CCTAE. Center for Aerospace Science and Technology. Lisbon, Portugal.

[(4)] AEROG, Aeronautics and Astronautics Research Center, Covilhã, Portugal.

[(5)] IDMEC. Institute of Mechanical Engineering, Lisbon, Portugal

where v_{stage} is the corresponding aircraft speed and D_{stage} is the aircraft drag. Knowing the duration of each stage, t_{stage}, it is then possible to calculate the propulsive energy required at each stage of the mission:

$$E_{req} = P_{req} \times t_{stage} \tag{3.2}$$

The total efficiency of the components is estimated as:

$$\eta_{state} = \eta_B \times \eta_C \times \eta_{ESC} \times \eta_{Mstage} \times \eta_{Pstage} \tag{3.3}$$

where η_B , η_C and η_{ESC} are the efficiency of battery, cable and electronic speed controller, common for all stage, and η_{Mstage} and η_{Pstage} are the efficiency of electric motor and propeller for the particular stage. Then the total required energy can be determined as:

$$E_{req} = \frac{P_{req}}{\eta_{stage}} \times t_{stage} \tag{3.4}$$

The best option to generate energy during cruise flight is to accommodate highly efficiency solar cells on the upper wing surface. The total energy required and the maximum electrical power required were used for sizing the propulsion system.Table 3.1 summarizes the values of required electrical power and energy for each segment of the mission:

Table 3.1 – Energy requirements for propulsion system [20].

Segment	η_{stage}	P_{req}/η_{stage} (W)	E_{req} (kJ)
Take-off	15.9	451.2	0.4
Climb	22.4	444.7	266.9
Cruise	38.2	46.7	1370.9
Descent	-	0	0

3.2 Aircraft Specifications

The aircraft dimension is important to produce a high performance design.It has to be large enough to accommodate all electronic but has to be capable of depoyment from small landing-fields.The conceptual design of the airframe has been concluded and some of the relevant UAV specfications are summarized in table 3.2 [20].

Tabela 3.2- Solar UAV specifications.

Parameter	Symbol	Value	Units
Wing mean chord	c	0.33	m
Wingspan	b	4.5	m
Wing area	S_{ref}	1.5	m^2
Take-off-weight	W	52.4	N

Beyond its aerodynamic purpose the airfoil shown in Figure 3.1 has an additional importance regarding its curvature. It is a significant factor when attaching the solar panels that have limited flexibility.

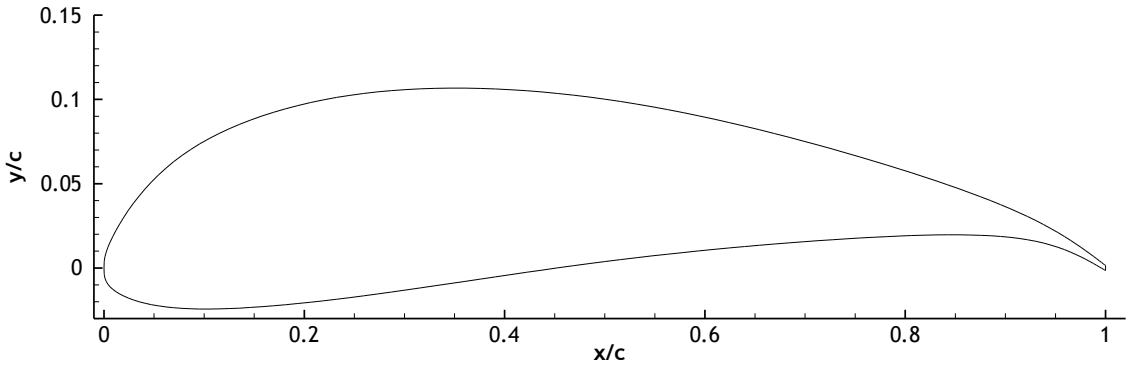

Figure 3.1 - 12% airfoil non-dimensional coordinates.

The solar cells are to be installed on the wing upper surface. Because of the limited flexibility of the solar panels to conform with the airfoil profile shape, and estimated area available S_{PV} was obtained using three correction factors applied to the wing reference area S_{ref}: curvature correction factor at the leading edge CF_{LE} (15 %), to account for the excessive curvature in this area; correction factor at the trailing edge, CF_{TE} (10 %), to account for the area occupied by the control surfaces; and wingspan correction factor, CF_W (18 %), to account for a safety zone at each wing tip:

This lead to the folowing available area for installation of the panels:

$$S_{PV} = C_{PV} . b_{PV} \tag{3.5}$$

where the available chord and available span are, respectively,

$$c_{PV} = \frac{100 - CF_{LE} - CF_{TE}}{100}.c \tag{3.6}$$

$$b_{PV} = \frac{100 - CF_{w}}{100}.b \tag{3.7}$$

resulting in an available area S_{PV} of 0.728 m^2 [21].

Additional information on the UAV performance data at different flight phases is given in, table 3.3.

Table 3.3- Summarized UAV estimated performance data.

Parameter	Value	Units
Take-off Speed	5.19	m/s
Climb Speed	6.67	m/s
Cruise Speed	7.5	m/s
Maximum rate of climb	2.2	m/s
Maximum Speed	21.1	m/s
Stall speed	6.1	m/s
Take-off Roll distance	8.1	m

3.3 Electric Propulsion System with Solar Energy

The aim of this project is to design an energy generation system able to provide a sustainable flight of 8 hours. However, the use of conventional methods for energy storage do not allow the storage of enough energy to sustain the model airborne over the course of the mission. For this particullary reason, an electric propulsion system powered by photovoltaic solar cells was planned. This system would be accomplished by joining an energy storage device and an energy production system. The energy accumulador would be a high density battery and the production system a solar array connected to a charge controller.
The top, front and side view of the UAV are shown in Figure 3.2 as well CAD rendering of UAV at figure 3.3.

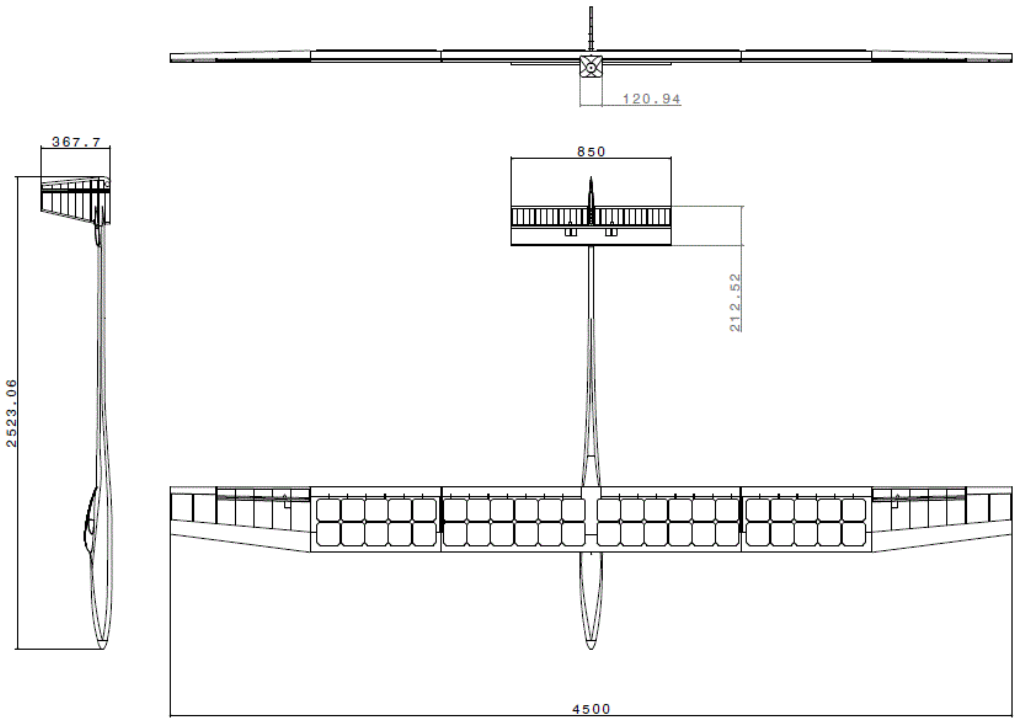

Figure 3.2 - CAD drawing views of UAV [21].

Figure 3.3- CAD Rendering of UAV [21].

Chapter 4

Solar Module, Solar Panel and Solar Array Arrangement.

In the outdoor environment the magnitude of the current ouput from a PV module directly depends on the solar irradiance and can be increased by connecting solar cells in parallel. The voltage of a solar cell depends primarily on the cell temperature. PV modules can be designed to operate at different voltages by connecting solar cells in series. This chapter aims to describe and justify each decision regarding the solar module arrangement.

4.1 Solar Panel

Sunpower C60 solar cells have been chosen to supply the photovoltaic effect needed.Figure 4.1 ilustrates these solar cells.

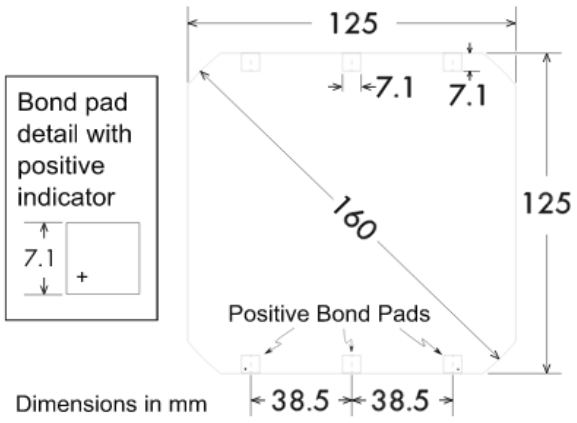

Figure 4.1- C60 Solar Cell and Bond Pad Dimensions [22].

The module is encapsulated with a polymer encapsulant on the front side and a polymer backsheet, which protects and gives strength to the cells and allows easy mounting of the panel. The edges are sealed for weatherproofing. For large power applications, as in this case, the PV modules are connected in series.

4.1.1 Efficiency

The solar cell efficiency is defined as the ratio of energy output from the solar cell to input energy from the sun. The energy conversion efficiency ($\boldsymbol{\eta PV}$) of a solar cell is the percentage of the solar energy to which it is exposed that is converted into electrical energy. This is calculated by dividing a cell's power ouput (in watts) at its maximum power point ($\boldsymbol{Pmax}$) by the input light irradiance (W/m^2), ($\boldsymbol{Imax}$) and the surface area of the solar cell ($\boldsymbol{A}$). Expressed as:

$$\eta PV = \frac{Pmax}{Imax \times A} \tag{4.1}$$

4.1.2 Current and Voltage Solar Cell

The typical I-V curve of a solar cell has a very characteristic shape. When the cell pads are not connected, no current is produced and the voltage equals to $\boldsymbol{V_{OC}}$, the open circuit voltage. When it is short circuited, the voltage is zero but the current equals to $\boldsymbol{I_{SC}}$. In between these two points there is a working point, called the maximum power point, where the power is the highest value possible and equals to:

$$Pmax = V_{MPP} \times I_{MPP} \tag{4.2}$$

It is exactly at this point that the cells should be operated and the ratio between $Pmax$ and the light intensity represents precisely the efficiency of the solar cell. However, the curve, and thus this point, is not fixed and varies depending on temperature and irradiance values.

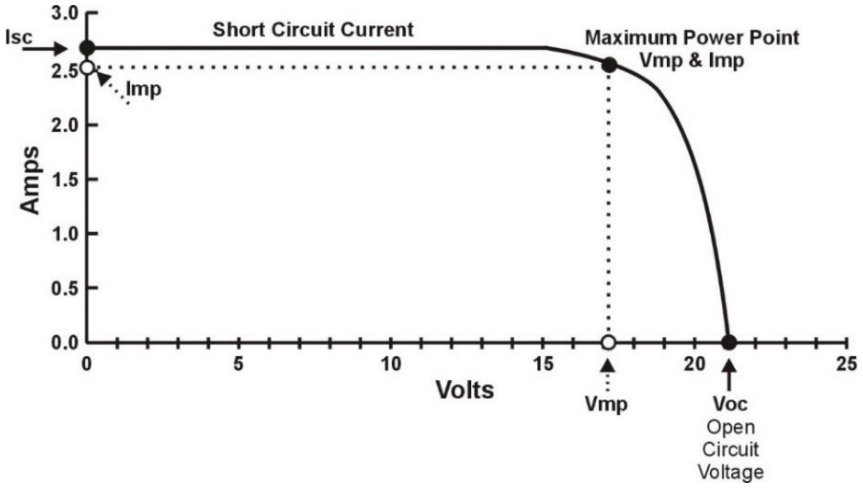

Figure 4.2- Example of an I-V curve characteristcs of PV module [23].

The charge controller is used as an electronic device that varies the electrical operating point of the solar array to extract the maximum power possible, called, MPPT. As shown in Figure 4.3, the voltage and current typical efficiency curve depends on its irradiance (W/m^2).

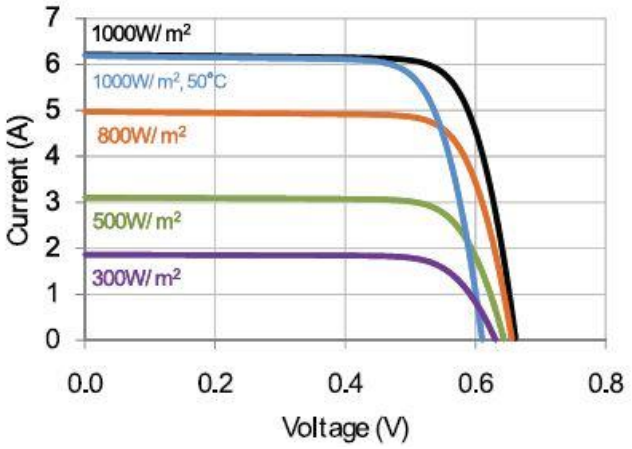

Figure 4.3-Sunpower C60 typical I-V Curve [22].

The current of a solar cell is proportional to its area and varies almost linearly with the light intensity. Like all semiconductor devices, solar cells are sensitive to temperature. The decrease in the band gap of a semiconductor with increasing the temperature can be viewed as increasing the energy of the electrons in the material. Lower energy is therefore needed to break the bond. In the bond model of a semiconductor band gap, reduction in the bond energy also reduces the band gap. Therefore increasing the temperature reduces the band gap. In a solar cell, the parameter most affected by an increase in temperature is the open-circuit voltage. The impact of increasing temperature is shown in the figure 4.4 [24]. Chapter 7 shows a detailed study on the temperature effect of the selected solar cells.

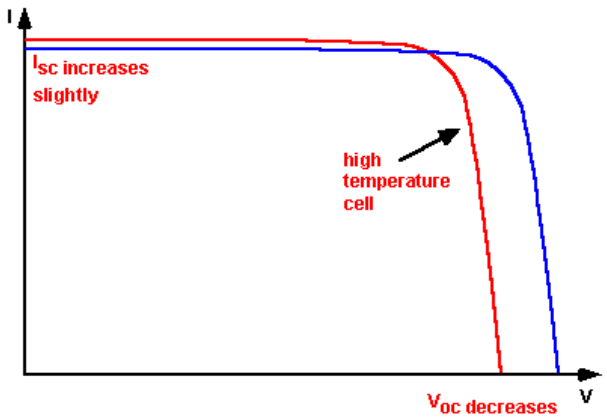

Figure 4.4- Effect of temperature on the I-V characteristics of a solar cell [24].

4.2 Solar Array

Components of an electrical circuit can be connected in many diferent ways. The two simplest of these are called series and parallel. Components connected in series are connected along a single path, so the same current flows through all components and the voltage increases. Components connected in parallel are connected so the same voltage is applied to each component, and the current increases. Sunpower C60 solar cells' typical electrical characteristics standart test conditions are given in table 4.1:

Tabela 4.1- Electrical characateristc of a typical cell C60 at standard test conditions (STC) [22].

Electrical Characteristics of Typical cell at Standard Test Conditions (STC) **STC:1000 W/m^2, AM 1.5g and Cell Temperature 25°C**						
Bin	P_{MPP} **(Wp)**	$Eff.$ **(%)**	V_{MPP} **(V)**	I_{MPP} **(A)**	V_{OC} **(V)**	I_{SC} **(A)**
G	3.34	21.8	0.574	5.83	0.682	6.24
H	3.38	22.1	0.577	5.87	0.684	6.26
I	3.40	22.3	0.581	5.90	0.686	6.27
J	3.42	22.5	0.582	5.93	0.687	6.28

Sunpower C60 solar cells have a maximum of 22.5 % [22] rated efficiency and an area of 0.018 m^2 per cell. The solar array consists of four modules of solar cells. Two modules of twelve photovoltaic cells and two modules of ten photovoltaic cells, all connected in series, Table 4.2:

Table 4.2- Solar Panel characteristics.

Parameter	**Mass (g)**	**Dimensions (mm)**	**Quantity (cells)**
Individual cell	14	130 × 135	1
2 × **5 solar array**	124.9	256 × 640	20
2×**6 Solar arry**	147.3	256 × 766	24
Total	544.4	-	44

The total area amounts to 0.72 m^2, which at the rated efficiency should ouput 151.8 W at maximum irradiation ground level of 1000 W/m^2 at 25° C. Since a single solar cell produces a nominal voltage of 0.582 V, Table 4.1, and the propulsion system will work at 12 V, at least 22 solar cells connected in series, V_{PV} = 0.582 × 22 = 12.80 V, are required. Since the Rated battery output current is 10.5 A and the recommended maximum V_{OC} at STC is 27 V it was decided that the four modules could be connected in series and therefore facilitate the wirring between the solar arrays. We first start by multipling the 0.582 V by 44 solar cells to obtain the solar panel maximum nominal voltage:

$$Panel\ V_{OC} = 0.582 \times 44 = \ 25.6\ V \tag{4.3}$$

Since the solar charger has a maximum output of $27\,V$ the connections are within the maximum value. Following the same reasoning, the current of the solar panel connected in series will be 5.93 A.Therefore, multipling the solar panel maximum voltage with the current we obtain the maximum power ouput:

$$P_{max} = 25.6 \times 5.93 = \ 151.8\,W \tag{4.4}$$

The battery module seleced in this system is a Lithium Polymer rechargeable battery with a nominal voltage of 11.1 V. As the maximum recommended voltage at STC of the charge controller is 27 V, the rated battery voltage is 12 V and the maximum power ouput from the solar array is whithin the MPPT value and the system is compatible. Table 4.3 contains the characterics of the complete solar array arrangement in series:

Table 4.3 - PV module specification datasheet.

Parameter	Value	Symbols	Units
Module type	Sunpower C60	–	–
Solar cell type	Mono C-Si	–	–
Rated power	151.8	w_p	W
Rated Current	5.93	I_{MPP}	A
Rated Voltage	25.6	V_{MPP}	V
Short circuit Current	6.28	I_{SC}	A
Open Circuit Voltage	30.23	V_{OC}	V
Configuration	12	–	V
Total number of cells	44	–	–
Performance Warranty	25	–	years

4.2.3 Solar Cells Flexiblity

The solar panel flexibility has a major importance when conforming the airfoil curvature so its flexibitily is studied using a polynomial approximation and a second order differentiation. Figure 4.5 shows the 12 % airfoil upper wing surface.

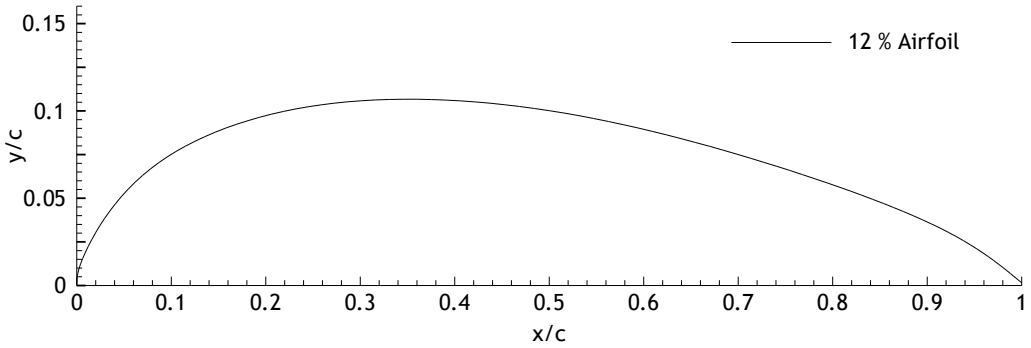

Figure 4.5- Upper Wing Surface using non-dimensional coordinates.

The second derivative of a function is the derivative of the derivative of that function which represents the curvature. We write it as $p''(x)$ or as $\frac{d^2p}{dx^2}$ and it studies the rate of change of a continuous function. To deduce the second order equation a sixth degree polynomial approximation is used.The objective is to obtain an approximation as close as possible to the actual function. This is accomplished by using the polynomial of high degree, as shown in Figure 4.6. The equation obtained is:

$$p_6(x) = -5.8056x^6 + 18.643x^5 - 23.66x^4 + 15.195x^3 - 5.4797x^2 + 1.1009x + 0.0078 \qquad (4.5)$$

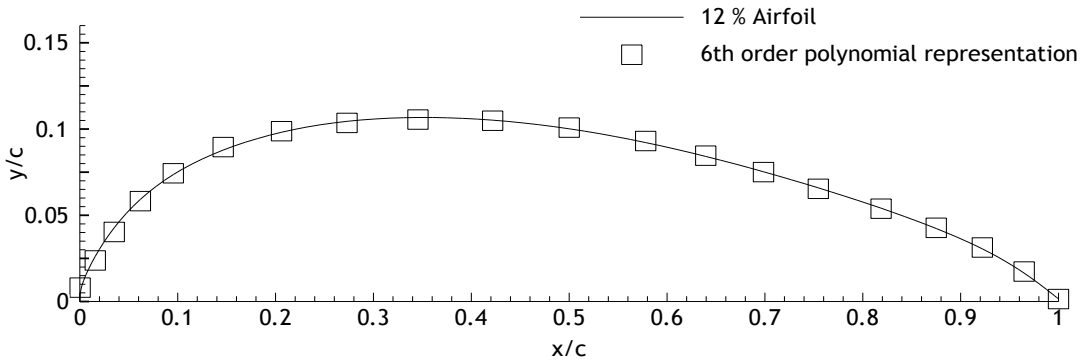

Figure 4.6- Sixth degree polynomial approximation.

The first derivative gives:

$$p'_6(x) = -34.8336x^5 + 93.215x^4 - 94.64x^3 + 45.58x^2 - 10.9594x + 1.1009 \quad (4.6)$$

and the second,

$$p''_6(x) = -174.168x^4 + 372.86x^3 - 283.92x^2 + 91.17x - 10.9594 \quad (4.7)$$

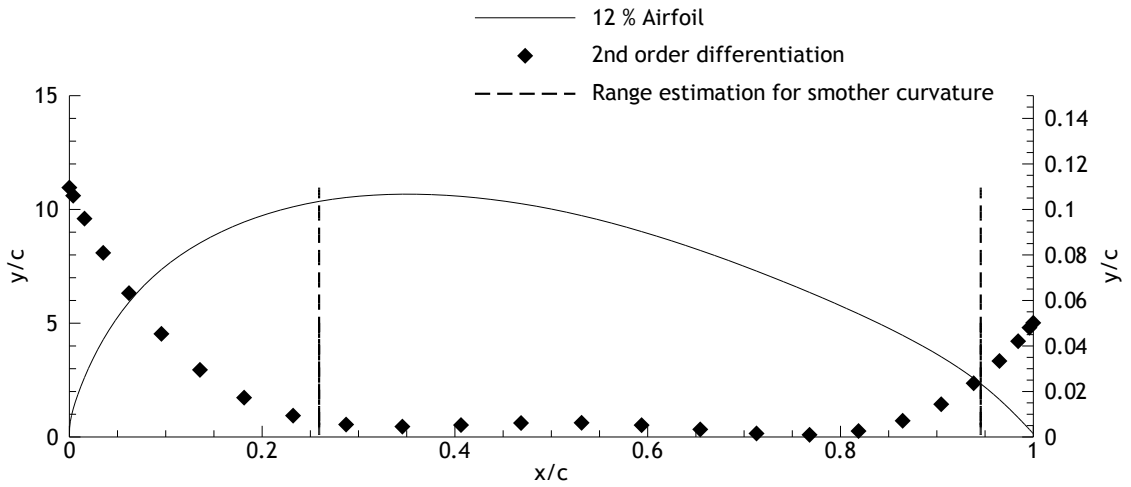

Figure 4.7- Second order differentiation with non-dimensional coordinates.

The range defined between the two straight lines in Figure 4.7 corresponds to the data range estimation for smother curvature. Laminar flow tends to occur at lower velocities therefore the airfoil disruption caused by the solar module should be placed as far back from the leading eadge as possible. Figure 4.7 shows that the solar panels should be placed at 1.5 cm from the trailing edge affect the aerodynamics of the airfoil as little as possible and to easily conform to its curvature.

Two sets of twelve solar cells exact placement on the central module of the wing are shown in Figure 4.8 and 4.9.

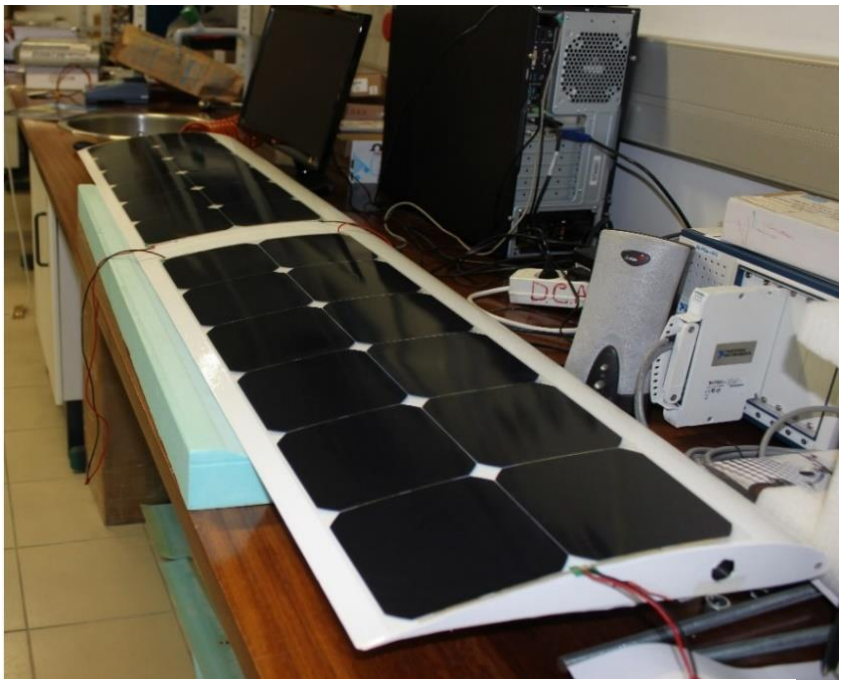

Figure 4.8- Solar panel placed on the central module of wing.

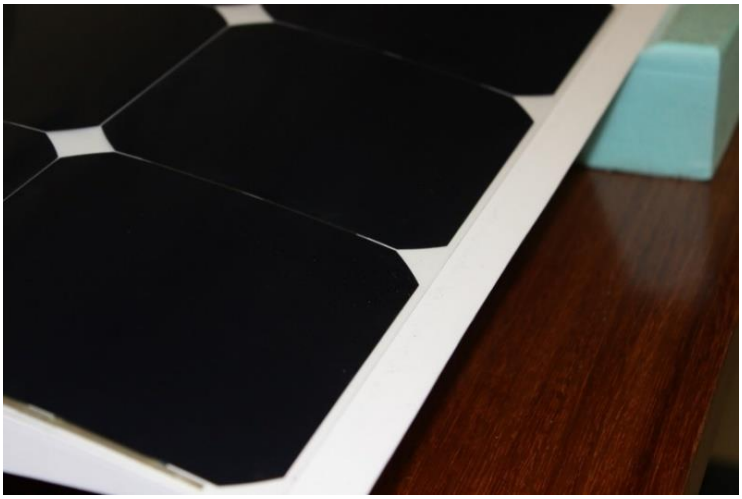

Figure 4.9- Solar panel placed at 1.5 cm from the trailing edge.

Chapter 5

Propulsion System Components, Electric Configuration and Installation on the Wing

Unmanned aerial vechicles are ideally suited for long endurance flights, but to be able to make full use of this feature, effective power sources need to be developed to ensure the long endurance functionality of the propulsion system and onboard equipment. The objective of this section is to describe each different component of the solar powered system and present the complete electric propulsion design.

5.1 Propulsion System components

A solar energy system that is properly installed and adequately sized will not require significant management. However, for those times of marginal sun or very large power requirements it is important to understand the relationship between the battery charge level, the amount of charge that they are receveing and the power being withdrawn from the system.Figure 5.1 shows the complete electric propulsion system scheme.

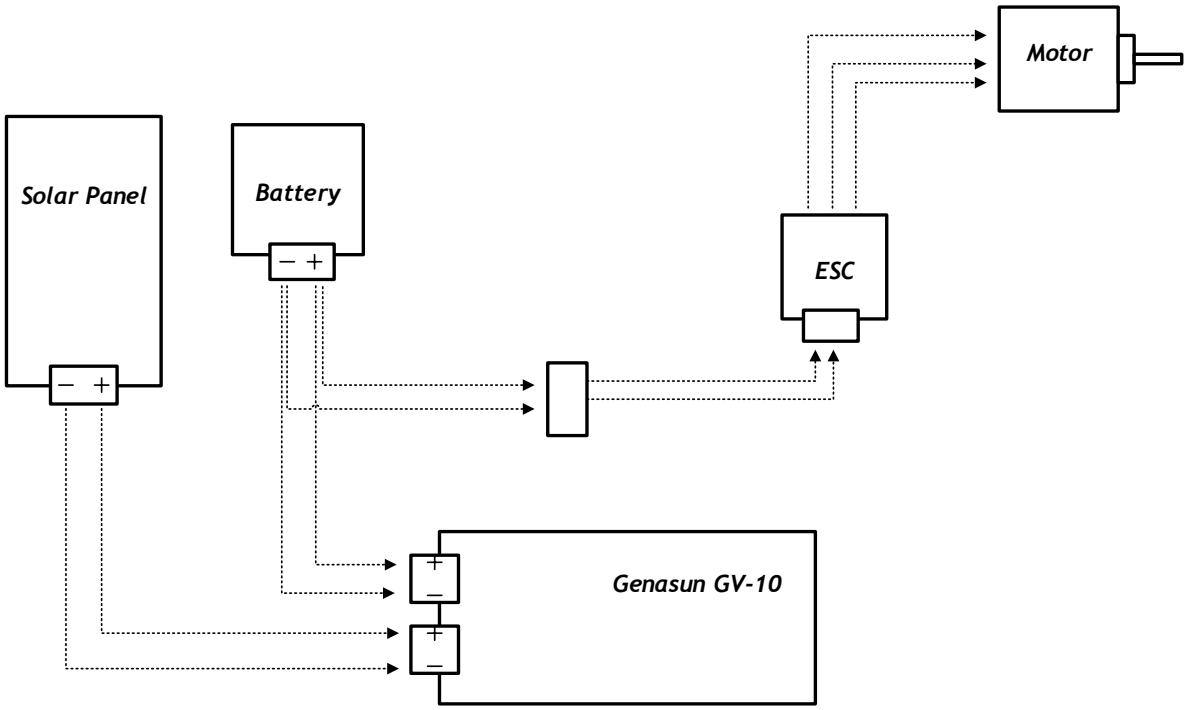

Figure 5.1- Electric Propulsion Configuration Scheme.

5.1.1 Solar Panel

For the solar array, Sunpower C60 Photovoltaic solar cells were chosen, figure 5.1. The anti-reflective coating and the reduced voltage provide exceptional energy delivery per power watt. Their innovative all back contact design moves gridlines to the back of the cell, which not only generates more power but also presents a more attractive cell design compared to conventional cells and a better surface for aerodynamic applications.

Figure 5.2- Sunpower C60 Photovoltaic Solar Cell [22].

The solar panel can be used as a component of a larger photovoltaic system to generate and supply electricity in specific applications. Because a single solar cell can produce only a limited amout of power, most installations contain multiple cells and e even panels. This project's system layout contains 4 solar panels with a total of 44 cells wired in series generatin 151.8 W with specific constraints.

5.1.2 Solar Charge Controller (SCC)

A charge controller monitors the battery's state-of-charge to ensure that when the battery needs charge-current it gets it, and also ensures the battery is not over-charged. Connecting a solar panel to a battery without a regulator seriously risks damaging the battery and potentially causing a safety concern. Charge controllers are rated based on the amount of current they can process from a solar array. If a controller is rated at 20 A it means that it is possible to connect up to 20 A of solar panel output current to this one controller. The most advanced charge controllers also include maximum power point tracking (MPPT) techonology. The charge controller chosen for LEEUAV Genasun GV-10, shown in figure 5.3.

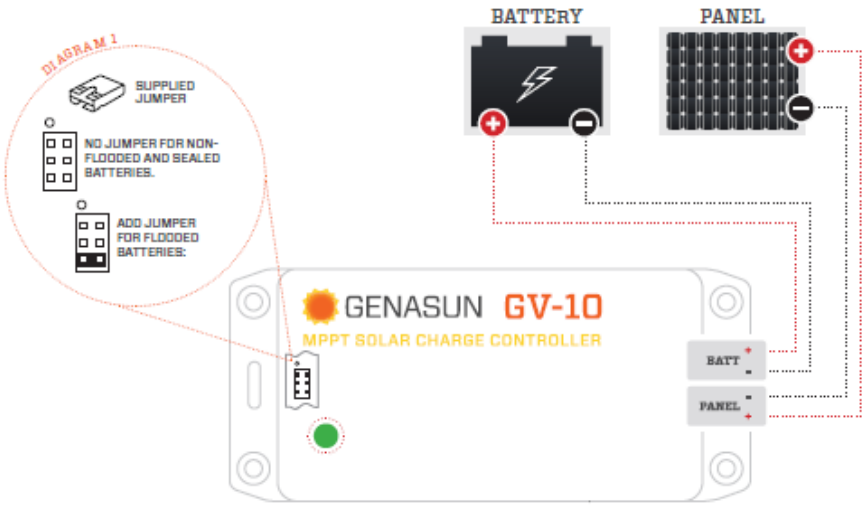

Figure 5.3- MPPT Solar charge controller Genasun GV-10 [25].

Maximum power point tracking is an electronic system that operates the PV modules in a manner that allows the modules to produce all the power they are capable of. MPPT is a fully electronic system that varies the electrical operating point of the modules maximizing the amout of current going into the battery from the solar array by lowering the panel's output voltage.

5.1.3 Battery

The electrochemical batteries are energy storage devices which are able to convert chemically stored energy into electrical energy during discharging. They are composed of cathode and an anode made of two dissimilar metals that are in contact with an electrolyte. When all elements are in contact with each other, a flow of electrons is produced. The chosen battery is LiPo (Lithium Polymer) and the main advantage of these batteries is its high discharge capacity and good specific energy. The battery that fits in this propulsion system is a 10,000 mAh 3S LiPo battery operating at a nominal voltage of 11.1 V.

5.1.4 Electronic Speed Controller (ESC)

An electronic speed controller works by applying full voltage to the motor, but turning it on and off rapidly. By varying the ratio of on time to off time, the speed controller varies the average voltage that the motor sees. Since at any given instant, the control is either fully off or fully on, this kind of control is theoretically 100 % efficient. In reality, electronic speed controllers are not 100 % efficient. Ignoring the factors introduced by switching rate the loss in efficiency is due to the fact the components doing the actual switching are not perfect.

They are not mechanical switches, and therefore have significant resistance. Whenever there is current flowing through a resistence, there is a power loss. When choosing the ESC it is necessary taking into acount the carrying current capacity, which is at least 65 A already established on the prelimany design of the LEEUAV. The selected ESC is Castle Creations Phoenix Edge model lite 100 A, supporting a maximum current of 100 A.

5.1.5 Electric Motor and Propeller

An electric motor uses electrical energy to produce mechanical work. The selection of a particular motor depends obviously on its application. Its choise has a major influence on the aircraft performance. The most important factor to consider is the power required for all mission phases and the energy consumption during the mission as a whole. Finding a combination of electric motor and propeller that matches a particular airplane and its desired performance is complex if done in an exact manner. The chosen motor is Hyperion ZS 3025-10 with a 13”x8” propeller.

5.2 Electric Configuration

5.2.1 Solar Panel- Charge Controller (Genasun GV-10)

Since the brigther the sunlight, the more voltage the solar cells produce, the excessive voltage could damage the batteries. A charge controller is used to maintain the proper charging voltage on the batteries. An American wire gauge conductor (AGW) is used to connect the components of the solar energy system, ensuring low loss of energy and preventing overheating. The AWG is a standardized wire gauge system for the diameters of round, solid, nonferrous, electrically conducting wire. The larger the AWG number or wire gauge, the smaller the physical size of the wire. The smallest AWG size is 40 and the largest is 0000. Since the maximum current ouput from the solar panel is 6A the AGW 20 was first chosen but due to its overheating and power losses a second choice led to AGW 12 with a length of 40 cm.

It can be observed in Figure 5.4 that the solar panels are connected to the input terminals of the charge controller, positive solar panel with positive charge controller and negative solar panel with negative charge controller.

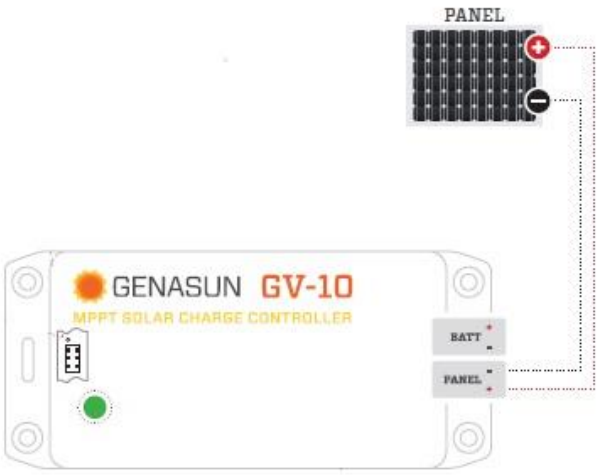

Figure 5.4- Solar Panel connect to the Charge controller [25].

5.2.2 Charge Controller-Battery

After connecting the solar panels to the input terminals of the charge controller, the same size wire can be used to connect the charge controller output to the batteries since these wires will carry no more current than the solar panel wires. The charge controller self protection feature will prevent damage from reverse polarity connections, but the charge controller will not function until the battery is connected properly (positive battery wire with positive charger controller and negative battery wire with negative charge controller).

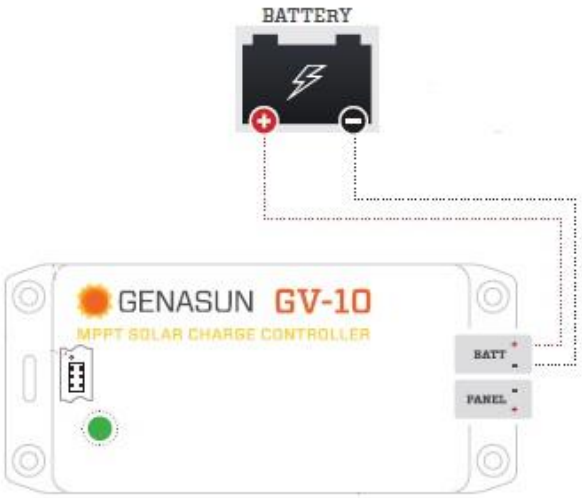

Figure 5.5- Charge controller connect with battery [25].

5.2.3 Battery-Motor

Once the battery is properly connected to the charge controller ouput terminals we must attach a battery connector, connect the motor to the ESC and, finally, the ESC to the receiver, performing the following steps:

1. **Battery connector**

   A battery connector will be attached (XT60 connectors) to the red (+) and black (-) power wires and then the battery connectorwill be soldered to the wires ensuring that the polarity is correct (red wire to battery red wire, black wire to battery black wire).

2. **Connecting Motor to ESC**

   Regarding the Motor-ESC connection it is necessary to solder the corresponding connectors (bullet connectors) for the motor to the wires coming from the ESC. It is important to ensure that the soldered joint is solid since poor soldering is a commom cause of failure.

3. **Connecting ESC to Receiver**

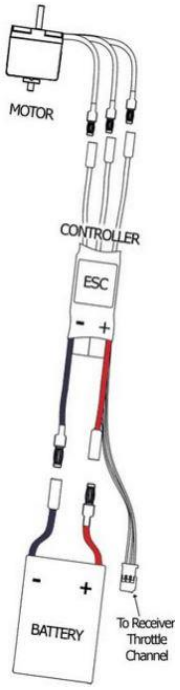

Figure 5.6- Battery- Mot

   The receiver lead (the brown/red/orange wires with a black plastic connector on the end) is connected to the throttle channel on the receiver.

5.3 Installation of the Solar Arrays on the Wing

With the solar cells being a critical part of the aircraft, their position has to be correctly planned to preserve the UAV balance, both on the ground and during flight. Since its fuselage is very thin and the four panel modules cover an area of around 0.72 m^2 the need to place the solar cells on the UAV wing is clear. Since the aircraft has to be small enough to deplete from small landing fields and be easily transported, the wing was divided in three parts, as seen in Figure 5.7.

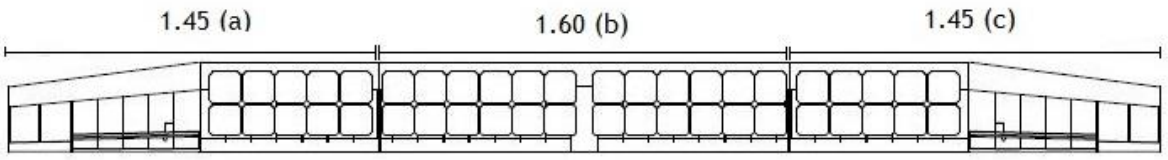

Figure 5.7- Solar modules integration view on the wing.

Module *(a)* and *(c)* are covered with a solar array of ten solar cells each one, and module *(b)* with two sets of twelve solar cells connected in series. The system consists of 44 solar cells with 544.4 g of mass wired in series (JST connecters from *(a)* to *(b)* and from *(b)* to *(c)*). On module *(b)*, the wiring between the two sets is completed using a bullet and a XT30 connecter to enable the connection whithin the solar array, the charge controller and the battery as can be seen in Figure 5.9.

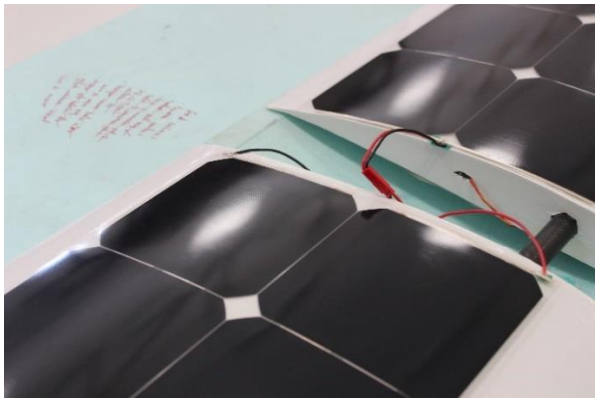

Figure 5.8- Module *(a)* and *(b)* wired with a JST connecter.

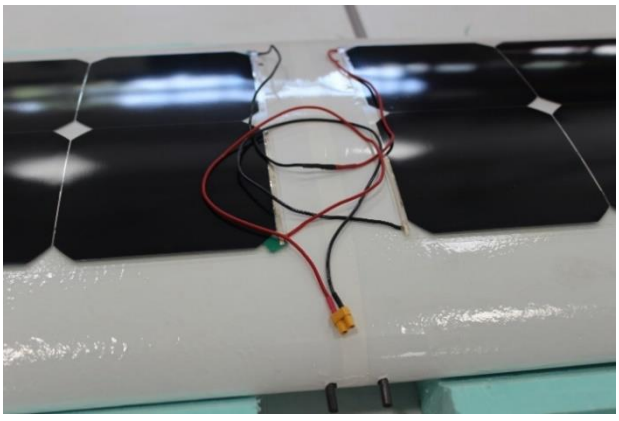

Figure 5.9- Module *(b)* wired with a bullet and a XT30 connecter.

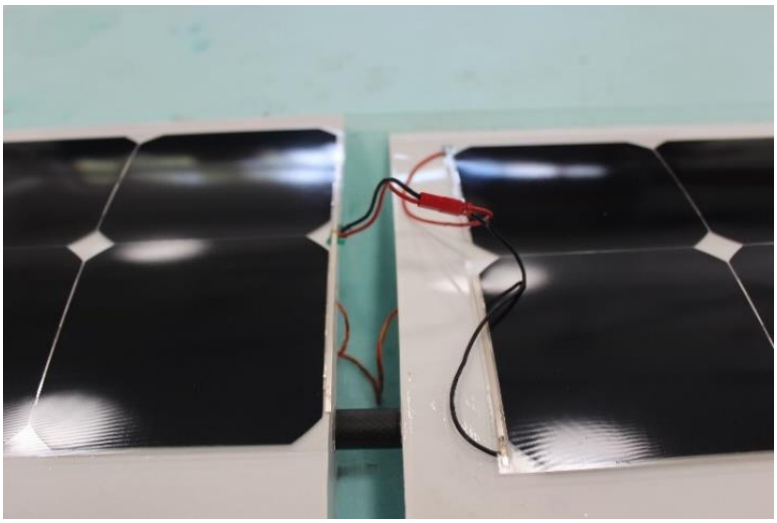

Figure 5.10- Module *(b)* and *(c)* wired with a JST connecter**.**

In these conditions, the solar UAV can accomplish a sustained flight of full eight hours during the summer months, being the battery recharged during flight. During the night time the system will be only powered by the battery. The system energy generation is compound by the solar module which is connected to the charge controller referred in section 5.2.1. The propulsion system consists of the Hyperion ZS 3025-10 electric motor powering a 13”x8” propeller and controlled by a Castle Creations Phoenix Edge ESC.

Regarding the attachement on the wing, placing the solar cells flushed with the wing’s upper surface enclosed by an anti-reflective coating on top offers multiple advantages, although, in the first instance it was decided to place them on the top of the wing upper surface for simplicity.The solar panels are directly attached with adhesive tape onto the shrink film that covers the whole wing, with a reinforcement on the ribs and trailing edge area.The four solar modules arrangement are shown in Figure 5.11.

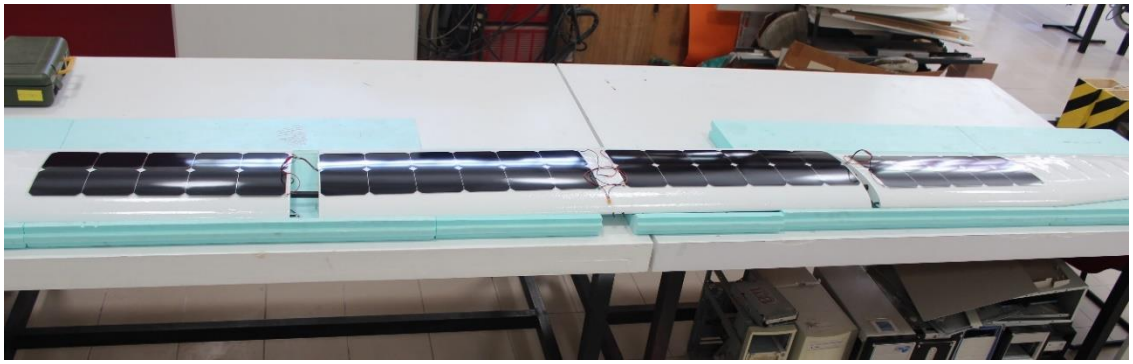

Figure 5.11- Solar Panel arrangement on the wing.

Chapter 6

Solar Arrays Experiments

This chapter aims to report the solar cells experiments that were carried out to measure the efficiency and compare with that given by the manufacturer of the selected photovoltaic solar cells. To validate the system the typical I-V curve was first built and then the efficiency was calculated using a variable load and a pyranomter.These steps are described in the following sections.

6.1. Pyranometer

A pyranometer is a device for measuring solar radiation on a normally flat surface. Measurement of solar radiation per unit surface area (W/m^2) is termed irradiance. Irradiance measurement requires, by definition, that the pyranometer's sensor response to radiation varies with the cosine of the angle of incidence from a line vertical to the surface of the sensor. The pyranometer used is the SP-215 Apogee, which means we can amplify the signal with a power source of no more than 24 VDC. According to the SP 215 Apogee manual [27] " Apogee Instruments SP series pyranometres consist of a cast acrylic diffuser, photodiode, and signal processing circuitry mounted in an anodized aluminum housing, and a cable to connect the sensor to a measurement device. Sensors are potted solid with no internal air space and are designed for continuous total shortwave radiation measurement on a planar surface in outdoor environments. SP series sensors ouput an analog voltage that is directly proportional to toal shortwave radiation from the sun. The voltage signal from the sensor is directly proportional to radiation incident on a planar surface (does not have to be horizontal), where the radiation emanates from all angles of a hemisphere."

6.1.1 Operation and Measurement

It is necessary to connect the sensor to a measurement device capable of measuring and displaying a voltage signal. In order to maximize measurement resolution and signal to noise ratio, the input range of the measurement device should closely match the ouput range of the pyranometer. It is also required to power the sensor with a DC voltage by connecting the positive signal to the white wire from the sensor and the negative or common to the clear wire from the sensor and to use a voltemer to measure across the green wire ouput signal and the clear wire. All apogee pyranometer models have a standart calibration curve [27].In this case the equation of calibration is:

$$Calibration\ Factor \times\ Sensor\ ouput = Shortwave\ Radiation \tag{6.1}$$

$$0.25\ W/m^2\ per\ mv\ \times\ mv\ = W/m^2$$

6.2 Solar Power Measurements

The solar experiments were conducted with a solar array of ten solar cells wired in series attached to the central module of the wing. In order to understand the behavior of the solar panel, a variable load is used. To simulate the electrical consumption of the motor, the choice led to three rheostats (connected in series) wired to a power meter and the solar array. Also, to help calculate the efficiency of the solar array, a pyranometer was used as mentioned previously. These experiments took place in Covihã during the summer months.

6.2.1 Solar irradiance measurement

Since the pyranometer used to measure the irradiation from the sun was internally amplified, a power source of no more than 24 VDC was required. At first, the power supply was a voltage source of 5 V connected to a bench multimeter but, in order to minimize the power losses, the power source went from a voltage source to a 2S LiPo battery connected to a multimeter with JST connectors, as shown in Figure 6.1.

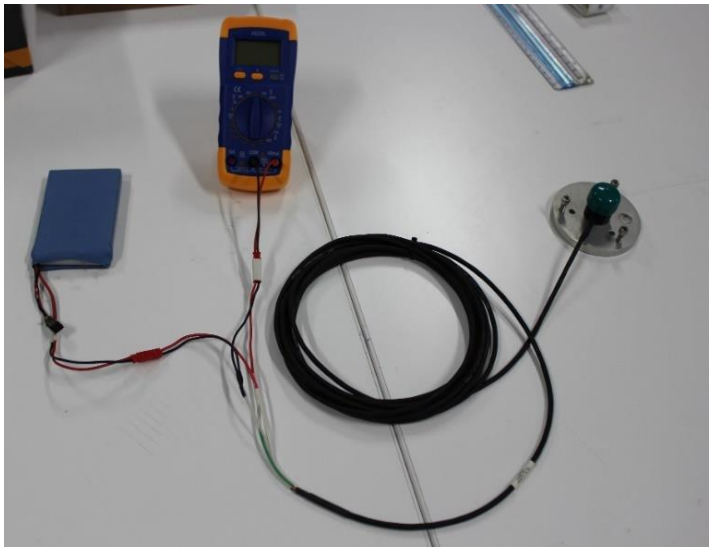

Figure 6.1- SP-215 Apogee pyranometer connected to a multimeter and a battery.

6.2.2 Typical I-V Efficiency Curve

The I-V (Current-Voltage) curve of a PV module describes its energy conversion capability at the existing conditions of irradiance and temperature. Conceptually, the curve represents the combination of current and voltage at which the PV module could be operated, if the irradiance and cell temperature could be held constant. Figure 6.2 shows different efficiency curves. The span of the I-Vcurve ranges from the short circuit current at zero volts, to zero current at the open circuit voltage. At both points the power generated is zero. V_{OC} occurs when the ouput current of the cell is zero, I=0 and the shunt resistance R_{sh} is neglected. The short circuit,I_{SC},is the current at V=0 and is approximately equal to the light generated current. At the 'knee' of a normal I-V curve is the maximum electrical power point (I_{MPP},V_{MPP}), the point at which the array generates maximum electrical power.

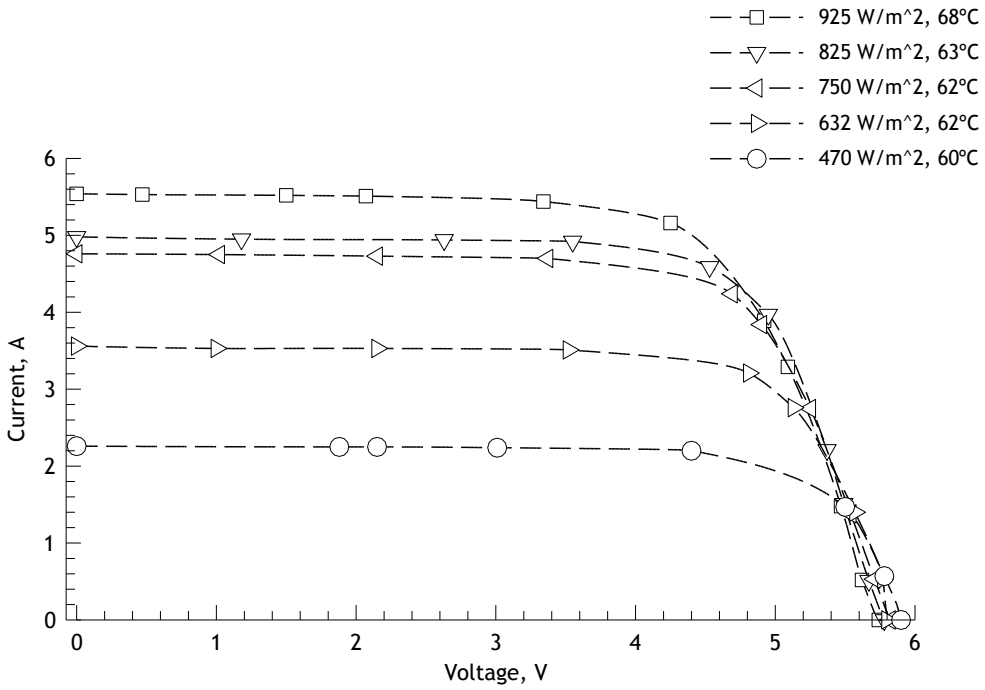

Figure 6.2- Efficiency I-V Curve at different Irradiance values.

In order to build the typical I-V efficiency curve three variable loads were used to simulate the motor electrical consumption and find the I_{SC} , maximum power point and V_{OC} values. When comparing these results with the typical I-V curve of Sunpower C60 datasheet the similarity is clear. Because the testing conditions are not as ideal as in the laboratory, average temperature of 36°C at ground level and non-controlled irradiance values, the obtained results are not as bright as shown in the datasheet. It is clear that

the irradiation is different throughout the day which means the irradiation at the beginning of the test is different from the irradiation at the end. The other reason for the difference between the curves is the fact that the manufacturer's curves were obtained at a controlled environment with STC conditions and these tests were conducted with the cell being heated by the sun making the solar array less efficient (detailed study in section 6.4).

6.2.3 MPPT working method

As previously explained, MPPT alghoritms are necessary in PV applications because the maximum power point of a solar panel varies with irradiance and temperature, so the use of a charge controller with MPPT techonology is required in order to obtain the maximum power from the solar array.

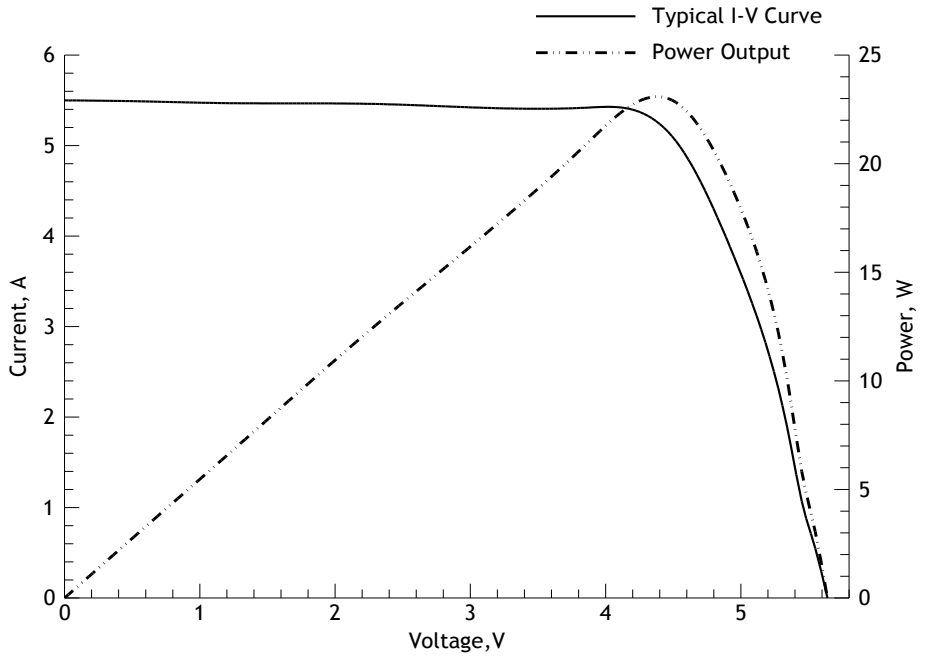

Figure 6.3- Power Output Evolution.

Assuming the solar panel conditions are 25ºC at ground level 1000 W/m^2 the entire solar system has a V_{MPP} of 25.6 V and an I_{MPP} of 5.93 A , $P_{max} = 151.81\,W$. Assuming that a 12 V battery may generally have 12.2V, the battery would charge $5.93\,A \times 12.2\,V = 72.35\,W$ which is significantly less than the maximum available output of the solar

module ($P_{max} = 151.81W$). The MPPT charge controller boosts[6] the voltage and the current of the voltage and current of the system close to the I-V curve maximum power point seen in Figure 6.3. Rather than simply connecting the module to the battery the MPPT system charge controller calculates the voltage at which the module is able to produce maximum power and forces the solar array to work always at the maximum power point.

6.3 Effect of transparent film Covering on Efficiency

A film covering study was conducted in order to understand the influence of the transparent film used to cover wings on the solar module efficiency. Solar array electrical parameters were recorded with and without the solar film covering the panel. The experimental test results are presented in Table 6.1.

Table 6.1- Results of the film covering experiments.

Azimuth 0º	**Irradiance (W/m^2)**	**Voltage (V)**	**Current (A)**	**Power (A)**	**Efficiency (%)**
Clean	882.5	4.39	5.12	22.5	15.9
Transparent Film	882.5	4.53	4.5	20.4	14.4
Azimuth 90º	**Irradiance (W/m^2)**	**Voltage (V)**	**Current (A)**	**Power (A)**	**Efficiency (%)**
Clean	907.5	4.52	5.04	22.8	15.7
Transparent Film	847.5	4.39	4.66	20.5	15.1
Azimuth 180º	**Irradiance (W/m^2)**	**Voltage (V)**	**Current (A)**	**Power (A)**	**Efficiency (%)**
Clean	862.5	4.52	4.66	21.1	15.3
Transparent Film	862.5	4.87	4.00	19.48	14.1
Azimuth 270º	**Irradiance (W/m^2)**	**Voltage (V)**	**Current (A)**	**Power (A)**	**Efficiency (%)**
Clean	820	4.33	4.15	18.0	13.7
Transparent Film	822.5	4.47	3.73	16.7	12.7

As it was expected, the solar cell covered with the film had their efficiency reduced but just slightly. There is an ouput loss ofaround 1% when covering the solar cells with the transparent

[6] **Boost**- Amplify an electrical signal.

film. As it is clear from Table 6.1, this efficiency loss would not affect significantly the aircraft performance, although, these experiments were conducted for a very short period of time and the effect over a long-term could be worst when the solar module heats up.

6.4 Effect of Temperature on Efficiency

Temperature also affects the characteristics of solar cells. When it increases, the voltage decreases whereas the current increases insignificantly. Globally, the power that a solar cell can give is higher for lower panel temperatures, considering the same irradiance conditions.

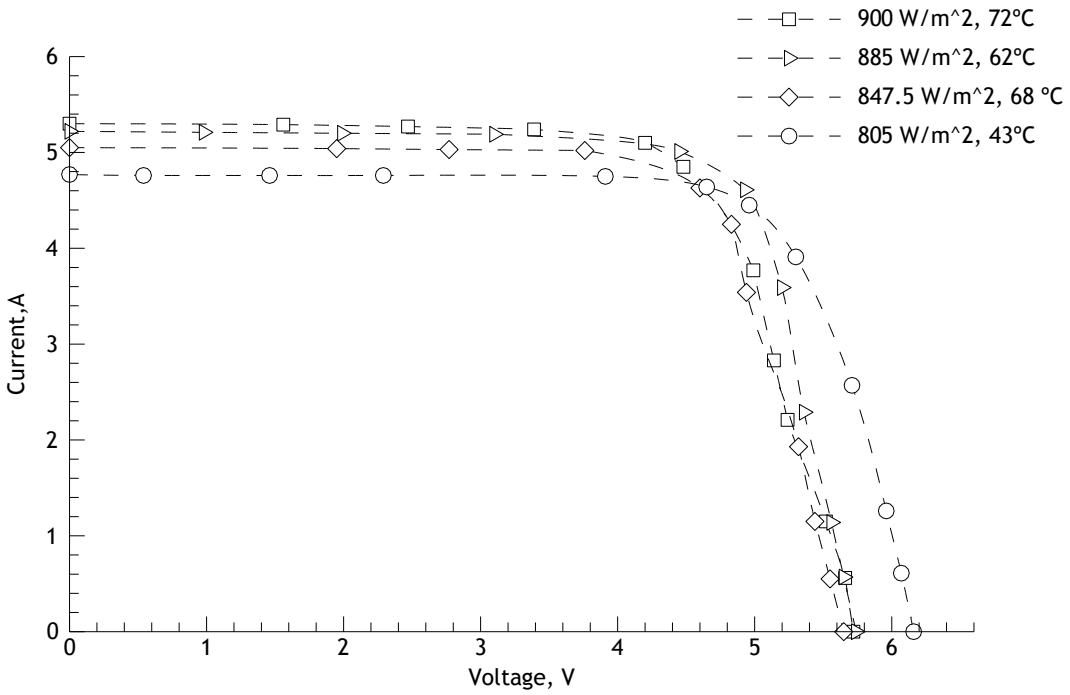

Figure 6.4- Variation of the current to voltage curve of a solar array with Irradiance and Temperature.

The experiments were conducted on a non-controlled environment, where Datasheet STC conditions could not be replicated. The first setback was the irradiance from the Sun. Since solar conditions change throughout the day, the irradiance at the beginning of the test is different from the irradiance at the end. Therefore, several experiments were conducted and various I-V curves were extracted (Figure 6.4.). Two samples of an I-V curve at different temperatures are shown in Figure 6.5.

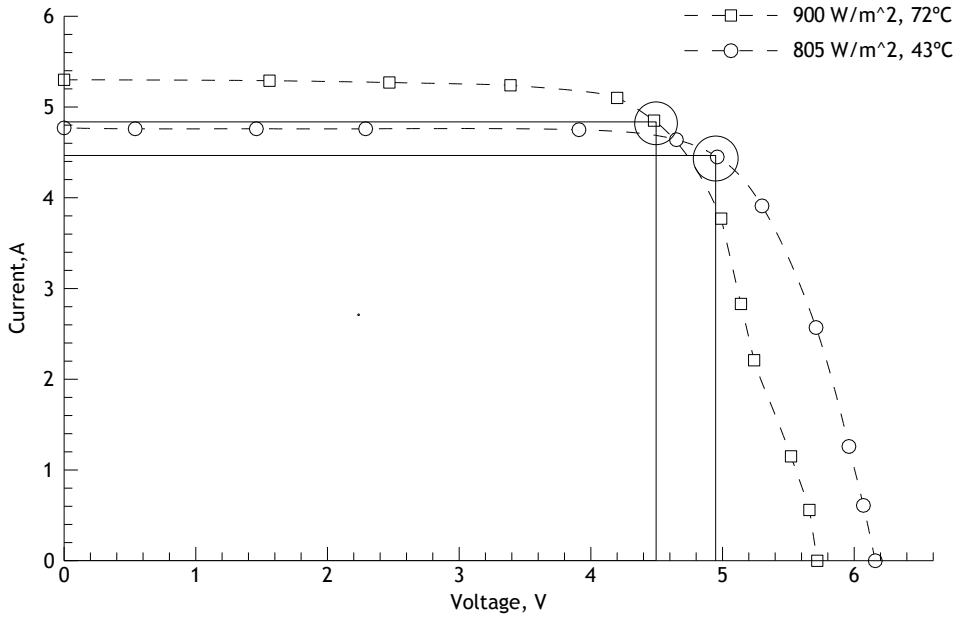

Figure 6.5- Two I-V curves at different temperatures.

To gather data for this chart, a PV panel was placed on the central module of the wing. The first measurements were taken in ambient temperature conditions, and then they were taken again after the panel was cooled with a fan. It can be concluded that the efficiency slightly decreases from its reference amount while temperature of the cell increases. The array will be heated up to 75ºC in a day average temperature of 36ºC when the cell is exposed directly to the sun, which results in loss of efficiency. However, the air flowing over the wing without a cover film decreases the temperature about 20ºC in less than 10 minutes at the speed of 2.8 m/s.Therefore, when the panel is at a higher temperature, a lower open circuit voltage is produced and the short circuit current increases insignificantly. The I-V curve with an irradiance value of 900 W/m^2 has a maximum power ouput of 21.5 W and the I-V curve of 800 W/m^2 an ouput of 22 W.

6.5 Solar angles-of-incidence

6.5.1 The Axes of Flight

Each axis of flight is an imaginary line around which an airplane can turn. Regardless of the type of aicraft, there are three axes upon which it can move: Left and Right, Forwards and Backwards, Up and Down. In aviation their technical names are lateral axis, longitudinal axis and vertical axis.

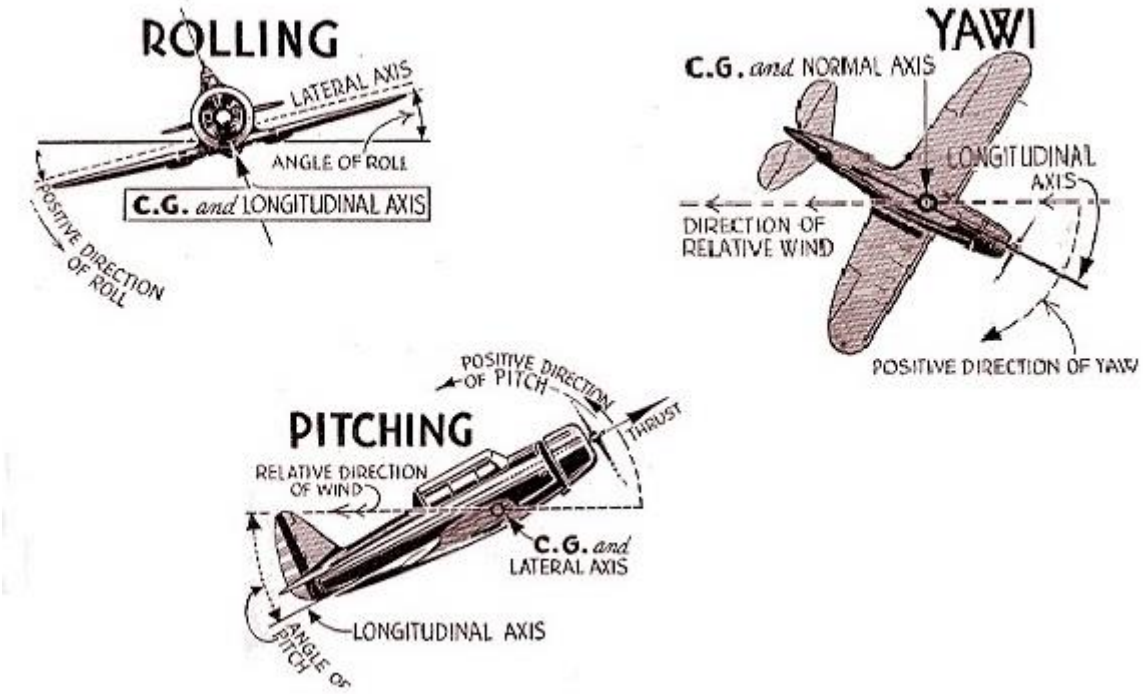

Figure 6.6- Aicraft Axes Flight illustration [28].

According to NASA "The yaw axis is defined to be perpendicular to the plane of the wings with its origin at the center of gravity and directed towards the bottom of the aircraft. A yaw motion is a movement of the nose of the aircraft from side to side. The pitch axis is perpendicular to the yaw axis and is parallel to the plane of the wings with its origin at the center of gravity and directed towards the right wing tip. A pitch motion is an up or down movement of the nose of the aircraft. The roll axis is perpendicular to the other two axes with its origin at the center of gravity, and is directed towards the nose of the aircraft. A rolling motion is an up and down movement of the wing tips of the aircraft."

6.5.2 Azimuth Angle

An azimuth is an angular measurement in a spherical coordinate system. The vector from an observer to a point of interest is projected perperdiculary onto a reference plane; the angle between the projected vector and a reference vector on the reference plane is called the azimuth.Azimuth is ussaly measured in degrees. Quite commonly, azimuths are stated in a system in which either north our south can be zero and the angle may be measured clockwise or anticlockwise from the zero. In our case the reference plane is the North.

6.5.3 Solar experiments

The change in the Azimuth angle during the day affects the power ouput of the PV module. One way to determine this would be to take measurements throught the day as the sun changed its angle relative to the panel module, but another way and easier to do is to roughly simulate the same effect by rotating the module in relation to the sun setting an initial position, in this case, north. While taking measurements it is important that irradiation readings be as constant as possible.To conduct these measurements the aircraft nose was placed towards North moving clockwise on a 360 degree circle, firstly horizontal and then combined with different pitch and roll angles. The experiment profile can be summarized as:

1. Location: Covilhã;
2. Aircraft initial position: Nose facing North, 0º Azimuth;
3. Irradiance values: Irradiance received at a ten solar cell module attached to a wing prototype central module;
4. Date: Mid-August, 2015;
5. Experiment duration: 14:30-16:00
6. Ambient temperature: 36ºC

The solar measurements started at 14:30 with an average temperature of 36 ºC. In these conditions the aircraft nose was placed facing north. At this time, the aircraft was facing the sun for this reason 0º azimuth has the highest power ouput value. All irradiance values taken during this experiment refer to irradiance receveid at the solar module (see Table 6.2).

Table 6.2 – Simulated Azimuth Angles.

Simulated Azimuth Angles	Irradiance (W/m^2)	Voltage (V)	Amperage (A)	Power Output (W)
0º	1200	4.59	5.51	25.3
45º	992.5	4.21	5.48	23.0
90º	925	4.25	5.16	21.9
135º	825	4.53	4.59	20.8
180º	855	4.76	4.84	23.0
225º	795	4.37	4.48	19.6
270º	772.5	4.97	3.82	19.0
315º	877.5	4.47	4.78	21.4

The experiment was conducted as quickly as possible, however the test still lasted 1 hour and 30 minutes, which means that the irradiance values were not as controlled as expected. Still, the values are consistent and it is possible to conclude that giving the airfoil curvature and position of the panels on the wing, according to Table 6.2, the north (0º azimuth) and south (180º azimuth) position are the most advantageous when it comes to enhace solar irradiance absorption, rising the available power ouput, Figure 6.7.These first measurements values refer to different angles of azimuth in relation to the sun with no influence of pitch and roll angles.

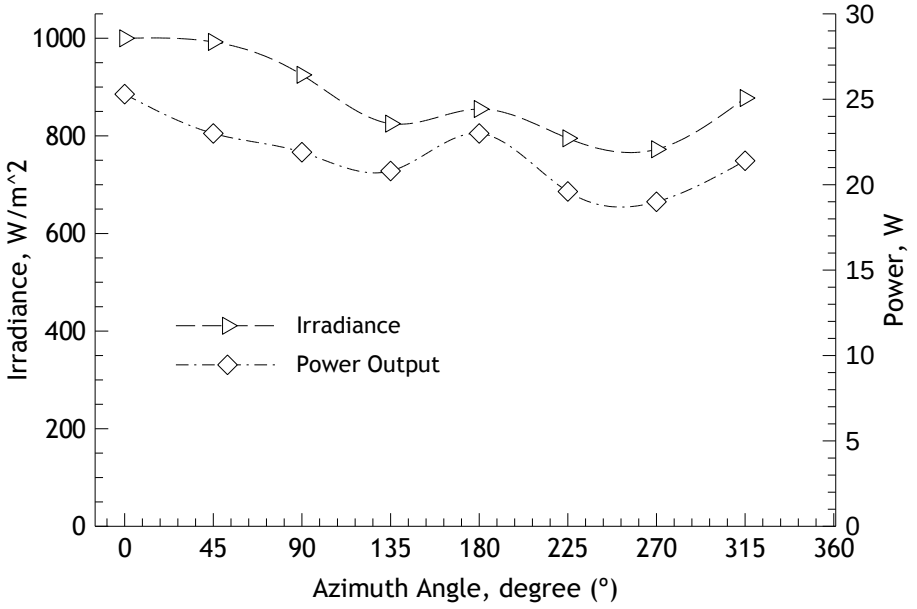

Figure 6.7- Influence of different azimuth angles on irradiance and power ouput.

As already refered, the first measurements were taken with the wing horizontal, not only to understand the azimuth effect on the power ouput but also to supply a base line when comparing these results to the influence of pitch and roll angles. The azimuth, pitch and roll angles are defined in the following graphis as A, P and R respectivelly.

According to the chart shown in Figure 6.8, an average of 2 % power loss was observed when the wing was moved on a pitch angle between 10º to 20º. However the roll angle had an insignificant influence in 0º azimuth. On the other hand, when comparing the results obtained in for 45º azimuth, Figure 6.8, there is an average of 3% power gain o when moving the wing on a pitch of 10º to 20º and a decline of 1 % in roll. This power ouput gain was expected since the irradiance from the sun arrives at a more perpendicular angle, reducing the losses from reflection. Regarding the 90º azimuth case, there is no major impact from a variation of pitch and roll. The most affected positions to a variation of picth and roll were 135º, 225º and 270º azimuth (Figures 6.9, 6.10, 6.11).

As the wing module suffers a variation of pitch from 10º to 20º the power ouput decreases 40%, however the roll angle variation approaches the availabe power ouput from its azimuth's original value.

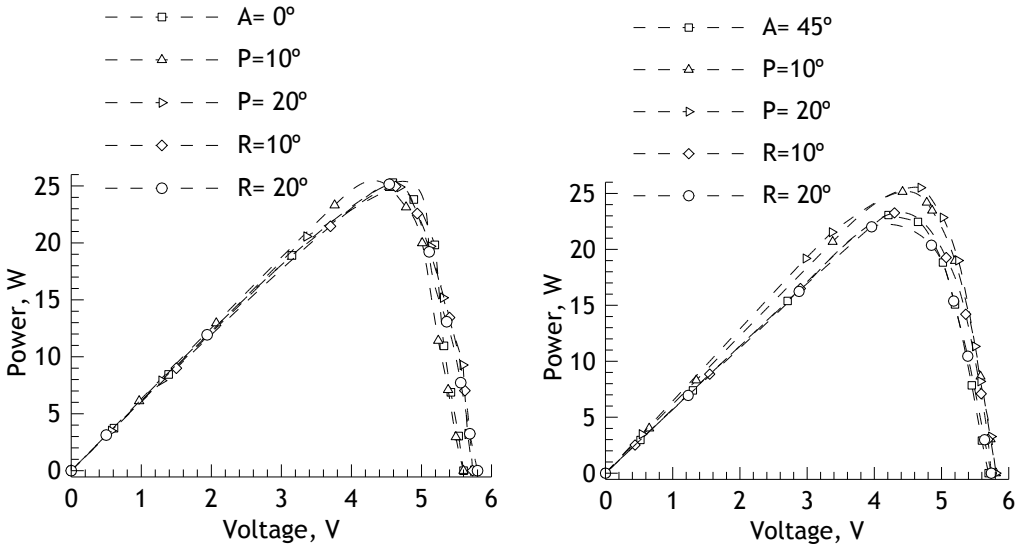

Figure 6.8- 0º and 45º azimuth with different combinations of pitch and roll.

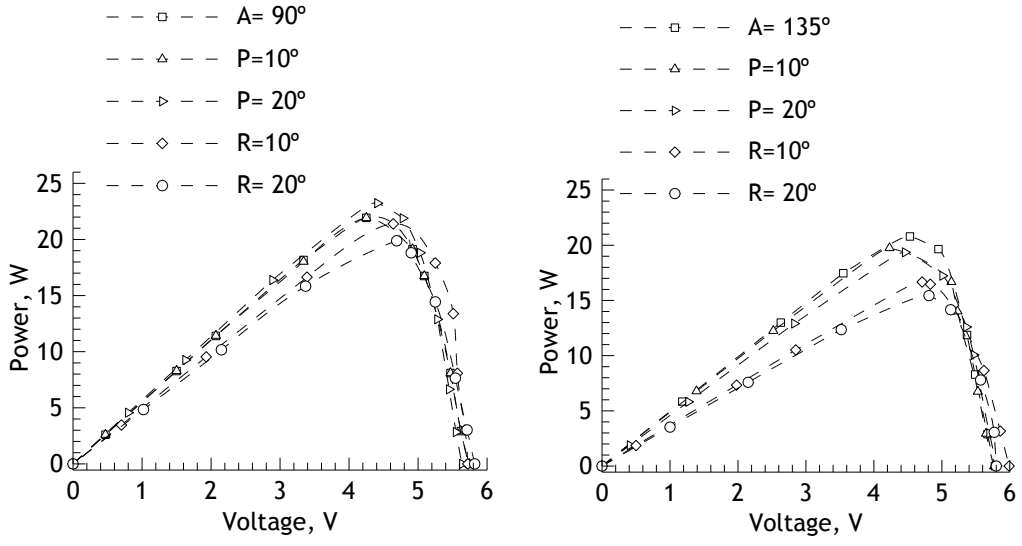

Figure 6.9- 90º and 135º azimuth with different combinations of pitch and roll.

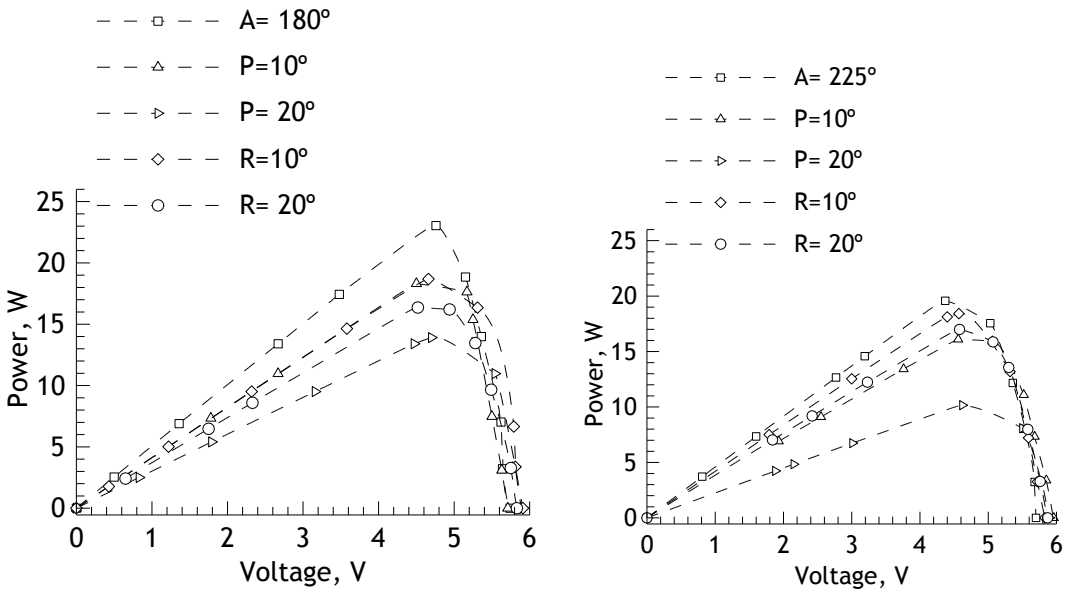

Figure 6.10- 180° and 225° azimuth with different combinations of pitch and roll.

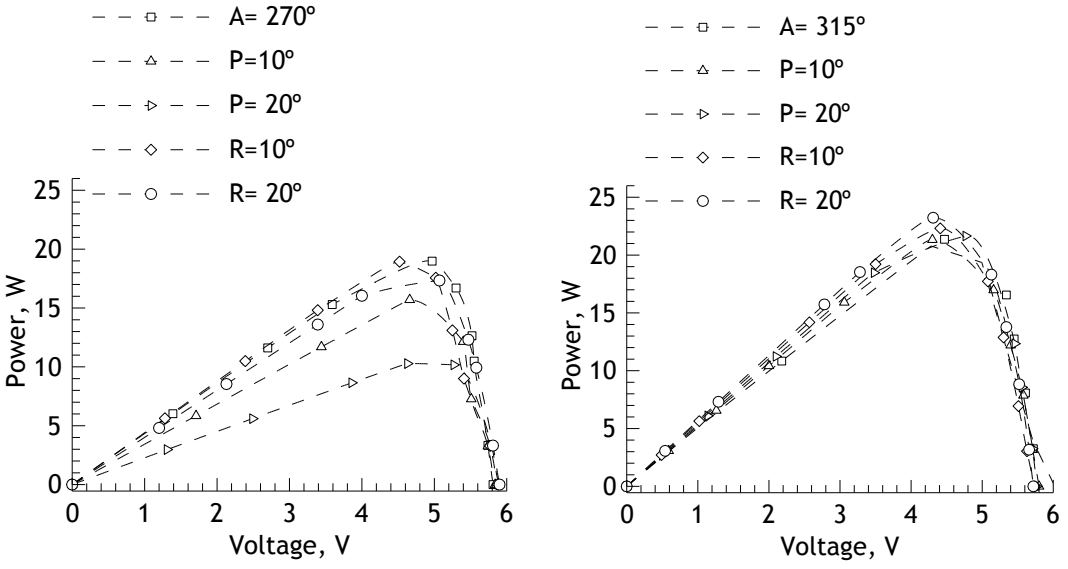

Figure 6.11- 270° and 315° azimuth with different combinations of pitch and roll.

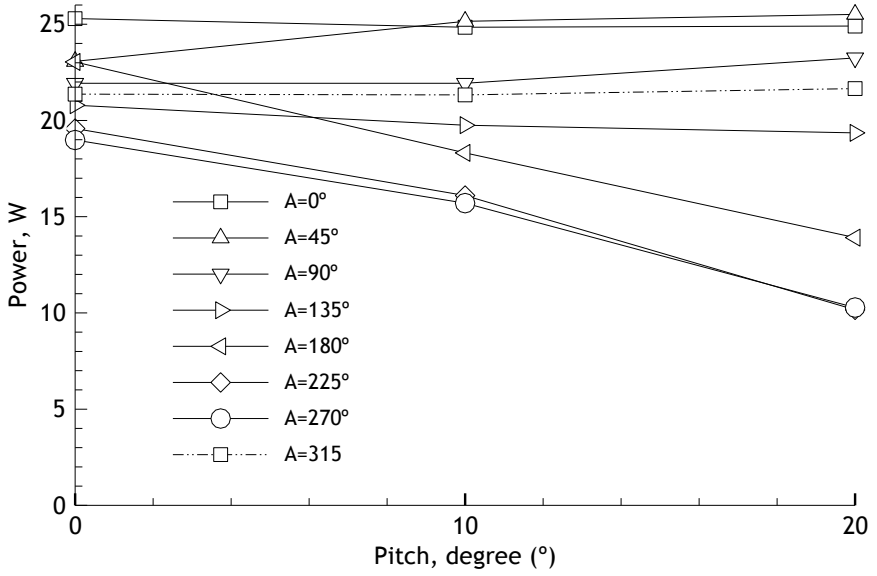

Figure 6.12- Pitch angle effect on power ouput.

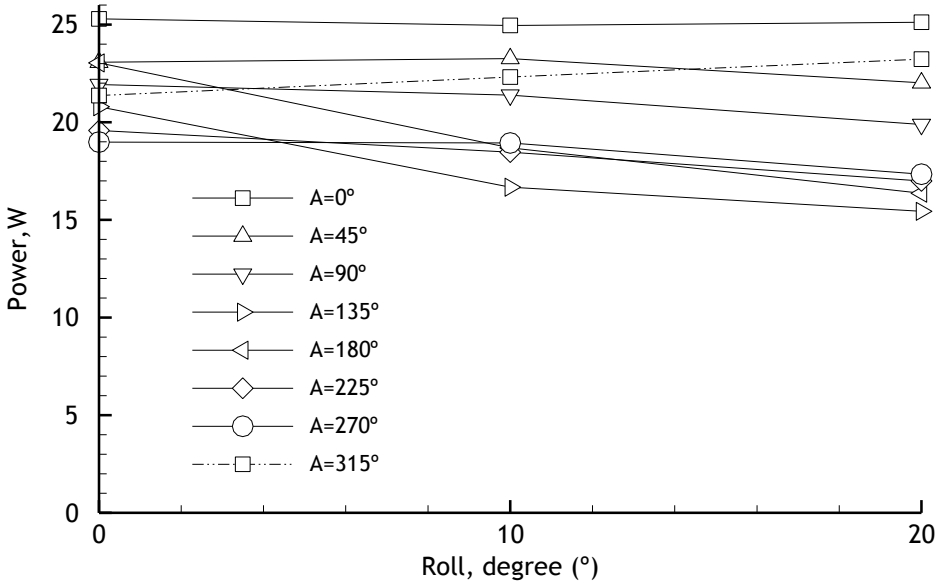

Figure 6.13-Roll angle effect on power ouput.

The power incident on a PV module depends not only on the power contained in the sunlight, but also on the angle between the module and the Sun. Experiments show that the phovoltaic system exact azimuth orientation is not critical. Vertical axis and lateral axis, given by pitch and roll, have a more important effect on performance. When the absorbing surface and the sunlight are perpendicular to each oher, the power density on the surface is equal to that of sunlight. Concluding, between 0º and 180º Azimuth, 91 % of the maximum energy is available moving north-east at several pitch and roll angles. Moving towards south-west systems are silghtly less efficient but whithin accepted level. Data collected shows that there is a 15 % power loss when moving towards west increasing the diffuse radiation and lowering the available power. Since this propulsion system is not a fixed solar panel on a roof or on an airframe fixed at a given place, any efficiency loss in the power output can easily be minimized by encouraging flying the aircraft in a pattern favouring a better attitude towards the Sun. Of course small variations in these values are not all problematic.

6.5.4 Loiter Pattern Simulation

By simulating a loiter pattern, an average power ouput during a possible aircraft surveillance mission can be determined. This simulation was done using the data from the graphis in section 6.5.3 and considering certain time intervals at each selected attitude. The profile simulation was defined as a land observation flight 1000 m long with an average cruise speed of 7.5 m/s and an altitude of 1000 m.Considering an eight hour loiter with several full laps an taking into account the variation of the solar irradiance due to sun position, a full lap duration is reached by:

$$d = t \times v \tag{6.1}$$

where d is the corresponding flight 1000 m long and v is the average cruise speed having t as 133.3 seconds. Therefore, if one lap corresponds to 133.3 seconds then 28,800 seconds (8 hour loiter) correspond to 216 laps. Considering that the perimeter of a circular turn is given by:

$$p = \frac{2 \times \pi \times v^2}{g \times \tan(\varphi)} \tag{6.2}$$

Then a half turn with v as 7.5 m/s and φ as 10º gives p=102.2 m and t=13.64 s.

As it can be seen from Figure 6.14, two basic types of mission segments are modeled: two steady-level cruise legs with 53 seconds each one and two turns with 13.64 seconds.

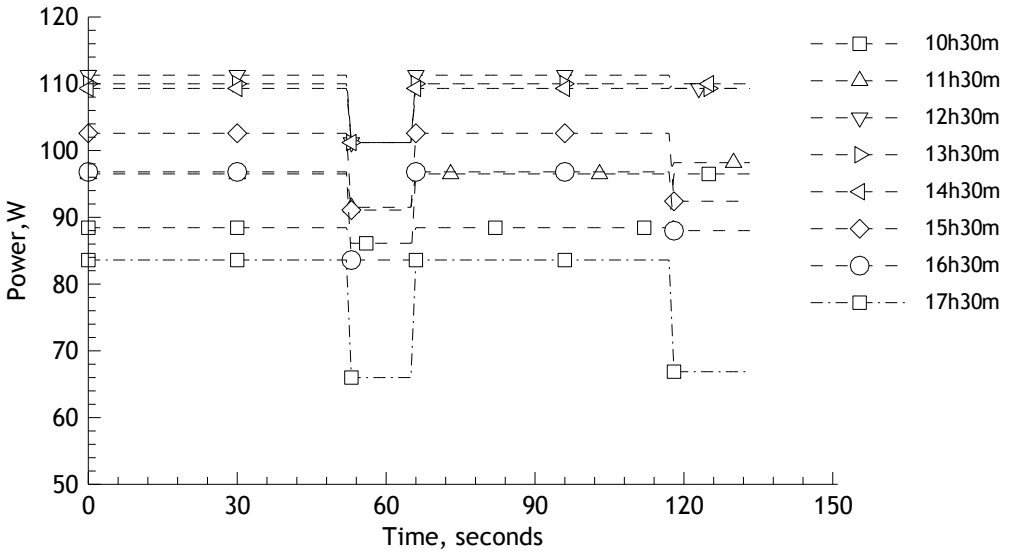

Figure 6.14- Loiter pattern simulation.

As already mentioned this simulation was done using the data from the graph shown in section 6.5.3 and assuming that radition emission from the sun remains constant for an hour, therefore, 8 different irradiance conditions were emulated. Notice that at the cruise speed of 7.5 m/s and 1000 m flight long, one hour corresponds to 27 laps and each turn has its characteristic average irradiance. Also, these experiements were conducted with a ten solar cell module, so, in order to obtain a power ouput from the complete solar array, it is necessary to convert the obtained available power value of a single solar cell and multiply it by 44 (44 solar cells wired in series).

The average irradiance at 10:30 in Covilhã is around 800 W/m^2 which gives an available power of 90 W. Until mid-day the irradiance values rises up to 1200 w/m^2 remaining almost constant during 2 hours, delivering 109 W. The lowest irradiance corresponds to 600 W/m^2, 60 W. So, taking into account that the MPPT's efficiency is 98% as given by the manufacter[22], the delivered average power output would be 93 W. Notice that the aircraft starts the loiter pattern facing north accomplished its first turn at second 65 towards east and the second turn at second 130.3 towards west. These values presented at figure 6.14 are an average power ouput.

Chapter 7

Mission Simulation

In order to validate the solar propulsion system a misson simulation was performed. The complete propulsion and data acquisition system were transported to the University of Beira Interior's wind tunnel where the take-off and cruise stage conditions could be replicated. Figure 7.1 ilustrates the wind tunnel used during the simulation.

Figure 7.1 – University Beira Interior's wind tunnel used during mission simulation.

Firstly the Hyperion ZS 3020-10 motor and 13"x8" propeller were attached to a vertical balance arm inside the wind tunnel, Figure 7.2. Once the motor and propeller were properly attached, the ESC was connected to the battery and the battery to the charge controller chosen, Genasun GV-10. Between the battery and charge controller a power log was placed to read the ouput power from the solar panel. The misson conditions were controlled inside a control room, where the thrust setting was adjusted according to each stage of the misson as well as the aircraft speed.

As already mentioned, a power log was placed between Genasun GV-10 and the 10,000 mAh LiPo battery to read the power output from the solar panel, as it is shown in Figure 7.3.

Figure 7.2- Mission simulation using wind tunnel.

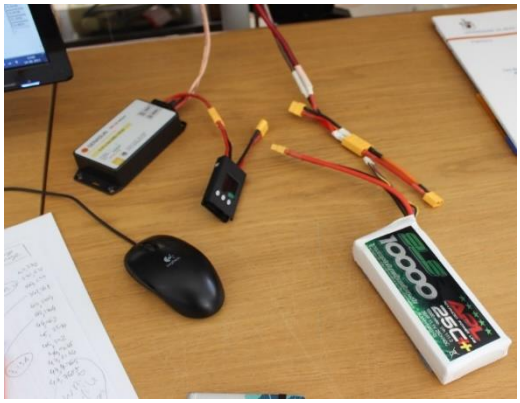

Figure 7.3- Power log placed between Battery and Charge Controller.

Finally, the solar panels were mounted on a wing prototype outside the wind tunnel, Figure 7.4. The simulation took place in Covilhã during the summer months, namely, end of August from 14:30 to 18:00 with the wing facing east. Once the complete propulsion and data acquisition system were placed on the appropriate place, the mission simulation started.The motor was run at full throttle for approximately 10 minutes with an average speed of 6.5 m/s and then reduced to nearly 50 W at a flight cruise speed of 7.5 m/s. It is important to understand that the sustainable-flight of full eight hours was not possible to replicate because sunlight only shows between 13:00 to 18:00 at the wind tunnel site given a total of 5 hours of solar irradiance.

Figure 7.4-Solar module attached to wing prototype for mission simulation.

During the climb phase observed in Figure 7.5 the electric power required is 411 W, below the expected. This is due to the mounting of the motor being inside of a wind tunnel and the conditions being considered ideal. The test began at 14:30 with a received solar irradiance of 880 W/m^2 which resulted in 90 W of solar panel power. It can be observed in Figure 7.5 that the power required during the climb phase is higher than the available power from the solar module. Therefore, the remaining required power will come from the battery, thus discharging it. On the other hand, during the cruise phase the power supplied by the solar array is higher than the power required by the motor, thus the excess power will charge the battery. These experiments were conducted in a place surrounded by mountains, therefore, the sun starts to disappear earlier and sunlight decreases abruptly, for this reason at minute 117 there is a significant drop in the power ouput from the solar module.

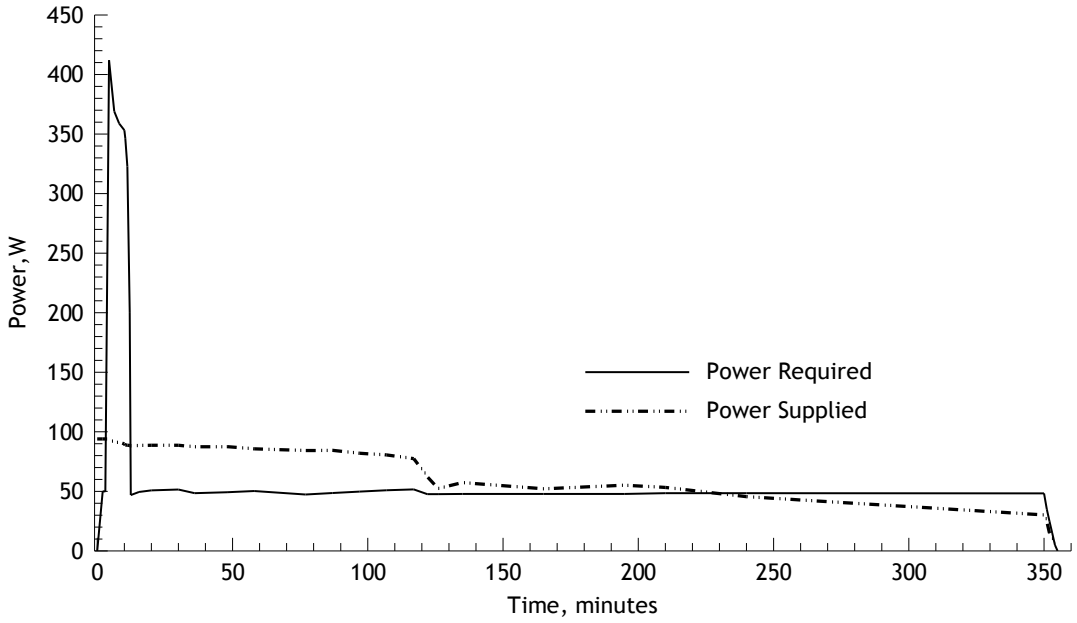

Figure 7.5 - Electric power required and supplied during mission simulation.

Using the Power curves in Figure 7.5 and the trapezoidal rule, the energy consumed during the climb phase, between minute 2 and 12, was calculated to be 189 kJ. It can be seen from Figure 7.6 that the consumed energy during climb corresponds to the energy peak existing in the graph being the total required energy and supplied energy 1174.10 kJ and 1249 kJ, respectively.

The batteries have a capacity of 10,000 mAh (432 kJ). During the climb phase the propulsion sub-system consumed 63 % of the available energy (6275.6 mAh, 259 kJ), without the solar input the remaining energy, at an average cruise power of 50W, would last for around 30 minutes.

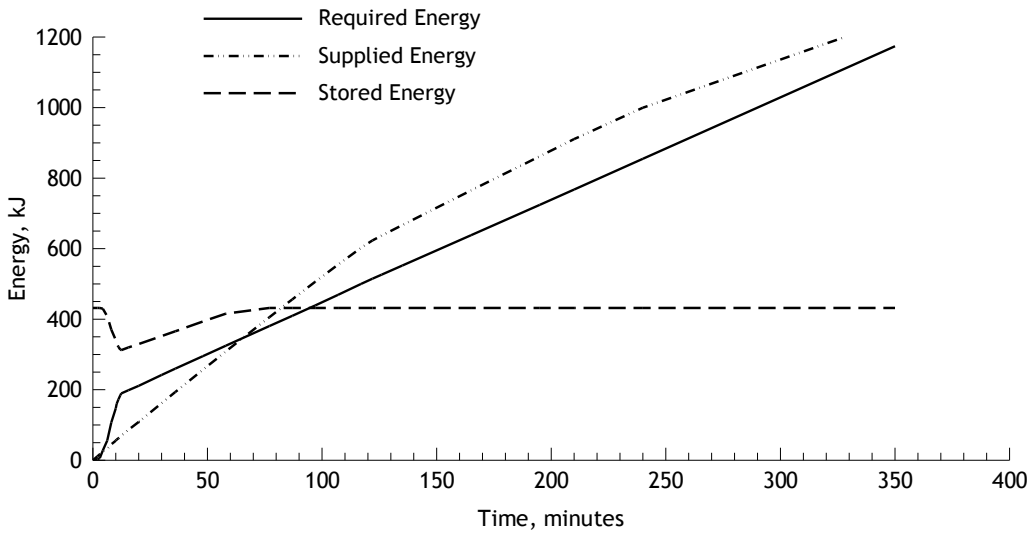

Figure 7.6- Consumed energy and supplied energy during mission simulation.

Although the simulation only lasted for 5 hours this does not mean that the sustainable flight of full eight hours plus climb is not possible. Using the irradiance values obtained over the last experiments conducted, a graph with the corresponding power ouput was built (Figure 7.7).

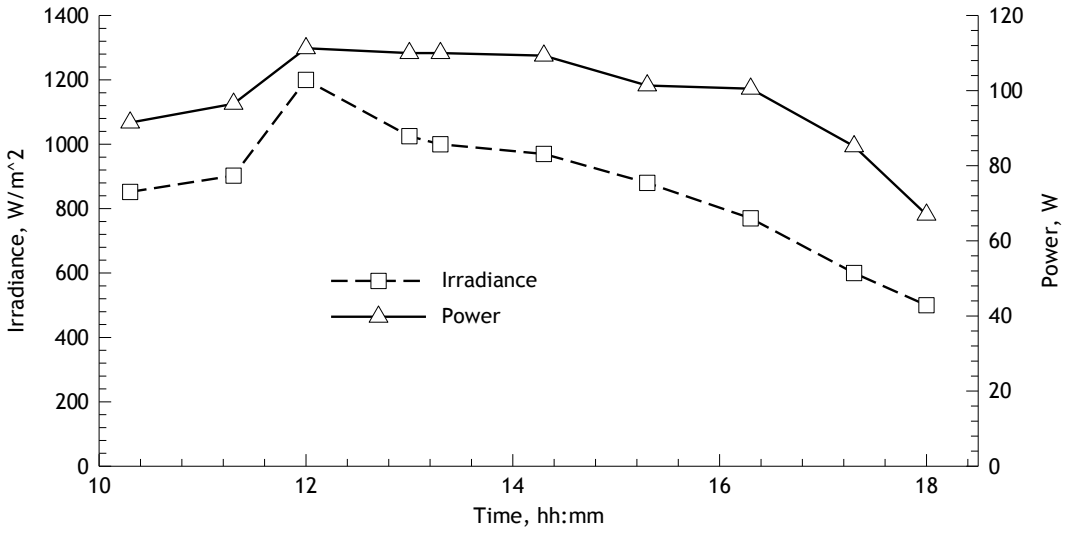

Figure 7.7- Irradiance values and power ouput according to day time.

Admitting the average sunlight of a normal day in Spring or Autumn equinox is 12 hours (sun rises at 07:00 and sets at 19:00) and the mission starts at 10:30, there would be 8 hours of

sunlight. Experiments conducted shows that the average irradiance at 10:30 in Covilhã is around 800 W/m^2 with 90 W at an ambient temperature of 35ºC (Figure 7.7). Until mid day the irradiance value rises up to 1025 W/m^2 meaning a power ouput of 111 W. If the climb phase consumes around 6,500 mAh, previously seen from the mission simulation, and with an average charge current of 2 A (solar array delivering 6 A and motor consuming 4 A) the battery will be fully charged in approximately 2 hours. Assuming ambient conditions are ideal, the motor will use direct energy from the solar module during 5 hours. Averaging 1 hour and a half power coming from the battery the mission could last for around 8 hours and a half.

Chapter 8

8.1 Conclusion

The purpose of this master thesis was to design a solar propulsion system for a long endurance electric UAV enabling a sustainable-flight of 8 hours during the Spring or Autumn equinox. Through this dissertation the mission was described along with detailed information about the energy requirements. Since this propulsion system is aimed at the use of green power technologies, the best option was focused on the use of high efficiency solar cells attached on the upper wing surface. The electric propulsion system is compound by the energy generation and storage systems, the solar module connected to the charge controller and a LiPo battery, respectivelly. The propulsion system consists on the Hyperion ZS 3025-10 electric motor driving a 13”x8”propeller and controlled by Castle Creations Phoenix Edge ESC. To verify the validity of this system, several tests were carried out.

To understand the power output from the solar module, the first step was to verify the efficiency I-V curves given by the Sunpower C60 manufacturer. To accomplish that, three variable loads and a pyranometer were used to measure the irradiance. Once the experiments were conducted and reviewed, it could be seen that the results obtained were very similar to the supplied manufacturer information. The only differences between these results were the non controlled environment of these performed experiments. The next step was to test the solar module efficiency loss due to solar cell temperature. As it was expect the solar power ouput is higher when solar cells are in a colder environment. Air flow through the wing during flight would decrease solar cell temperature resulting in a power ouput gain.

The power incident on a PV module depends not only on the power contained in the sunlight, but also on the angle between the module and the Sun, for this reason, some experiments to understand the contribution of azimuth, pitch and roll on power output were conducted. Experiments show that the phovoltaic system exact azimuth orientation is not critical. Vertical axis and lateral axis, given by pitch and roll, have a more important effect on performance.

Once the solar module behavior was understood throught different temperatures and irradiance values, a mission simulation was performed where the complete propulsion system and acquistion data system were installed in a wind tunnel. There were limitations at first since sunlight only strikes for 5 hours on the wind tunnel. However, the solar UAV accomplished his purpose with success, exhibiting sustainable flight of 5 hours. Despite the simulation only lasted for 5 hours this does not mean the full eigh hour sustainable flight can not be accomplished. When the power required by the motor is higher than the power supplied by the PV module the lacking power will come from the battery, thus discharging it. On the

other hand, during cruise the power supplied by the solar array is higher than the power required by the motor and the excess will charge the battery.

Although some limitations were found, this master thesis objectives were successfully achieved.

Concluding, important parameters which influence the ouput power and efficiency of PV cells should be taken into consideration for achievieng the desired performance in a solar-powered aircraft. Also, the type of covering and mounting of the cells affects the direct incident solar radiation, the amount of heat transfer on the wings and the ouput power. Due to air flow, temperature of the cells decreases during the flight and causes increased in efficiency. So this would be a significant factor while designing the aircraft, selecting the cells and covering the wings. Futhermore, this influences the weight, price and flight-endurance.

8.2 Future Work

In the future, a better and more accurate technique for placing the solar cells inside the wings will be studied.

References

1. Bone E, Bolkcom C. Unmanned Aerial Vehicles: Background and Issues for Congress. *Current*. 2003.

2. Bhattacharya S, Kumar S. Direct Solar Energy. *Energy Syst Direct Sol Energy,[Eds S]*. 2004:333-400.

3. Hersch P, Zweibel K. *Basic Photovoltac Principles and Methods*. United States of America: Tecnhical Information Office

4. Photovoltaic Solar Panel Working Principle. http://www.solarbuildingtech.com/Solar_PV_Tech/Images/PhotoVoltaic-solar-panel-working_princple.gif. Accessed April 12, 2015.

5. Aberle AG. Thin-film solar cells. *Thin Solid Films*. 2009;517(17):4706-4710.

6. Saga T. Advances in crystalline silicon solar cell technology for industrial mass production. *NPG Asia Mater*, 2010

7. U.S.Department of Energy. Photovoltaics: Tecnhnolgies, Cost, and Performance. In: *Sunshot Vision Study*, 2012:69-96.

8. NREL Efficiency Chart. http://www.nrel.gov/ncpv/images/efficiency_chart.jpg. Accessed April 12, 2015.

9. NREL. Solar cell efficiency explanatory notes. 2013.

10. Boucher R. History of solar flight. *AIAA Pap.*; Autonomous Systems Lab, Swiss Federal Institute of Technology Zürich, 1-7 July, 1984

11. Sunrise II. http://ecoble.com/wp-content/uploads/2009/02/sunrise-ii-astro-flight.jpg. Accessed April 12, 2015.

12. Pathfinder Solar Aircraft Over Hawaii. http://upload.wikimedia.org/wikipedia/commons/1/1a/Pathfinder_solar_aircraft_over_Hawaii.jpg. Accessed April 12, 2015.

13. Pathfinder Plus Solar Aircraft over Hawaii. http://upload.wikimedia.org/wikipedia/commons/6/68/Pathfinder_Plus_solar_aircraft_over_Hawaii.jpg. Accessed April 12, 2015.

14. Centurion. http://www.thenewecologist.com/wp-content/uploads/2010/09/centurion.jpg. Accessed April 12, 2015.

15. Helios. http://cdn.globalaircraft.org/media/img/planes/lowres/helios_2.jpg. Accessed May 8, 2015.

16. QinetiQ. http://www.qinetiq.com/media/news/releases/pages/zephyr-14-days.aspx. Accessed January 9, 2015.

17. Zephyr, 2010 Launch. http://theatlasgroup.biz/wp-content/uploads/2014/09/zephyr2010launch2.jpg. Accessed April 12, 2015.

18. Borshberg A, Piccard B. SOLAR IMPULSE. http://info.solarimpulse.com/timeline/view/7267#.VQHHx-Hw-AR. Accessed March 12, 2015.

19. Solar Impulse 2. http://www.arabiangazette.com/wp-content/uploads/2015/01/Solar-Impulse-2-1.jpg. Accessed April 12, 2015.

20. Cândido L., Projeto de um UAV Solar de grande autonomia. MSC Thesis, Universidade da Beira Interior, 2014.

21. Marta AC, Gamboa P V., Long Endurance Eelectric UAV for Civilian Surveillance Missions. *29th Congress of the International Council of the Aeronautical Sciences*, St. Petesburg, Russia, 7-12 September, 2014.

22. Sunpower Corporation.C60 Solar Cell Monocrystalline Silicon¸ November 2010.

23. Example of an I-V Curve. http://re.emsd.gov.hk/english/solar/solar_ph/images/redraw5.jpg. Accessed April 12, 2015.

24. Effect of Temperature | PVEducation. http://pveducation.org/pvcdrom/solar-cell-operation/effect-of-temperature. Accessed April 13, 2015.

25. Genasun,GV-10 Manual. Solar Charge Controllers with Maximum Power Point tracking, 2012.

26. Quality R/C Hyperion Products.http://www.allerc.com/motorwiring.htm. Accessed April 12, 2015

27. Apogee instruments,Inc.Owner's Manual Pyranometer Model Sp.212 and SP-215, 2013

28. Pitch, Roll and Yaw Axis. https://s-media-cache-ak0.pinimg.com/originals/34/21/16/342116988a06db33bfbffccb695badce.jpg. Accessed August 28, 2015.

Annex

Appendix A

Czochralski process – **"**is a technique for growing crystals in order to obtain solitary crystals of semiconductors like silicon, metals like silver and gold as well as several salts. The process is named after Jan Czochralski, who first demonstrated it in 1916. He was studying the rates of crystallisation of different metals. The most significant application of the Czochralski process is the growth of large ingots of single crystal silicon. Initially highly pure semiconductor-grade silicon is subjected to high temperatures in a crucible made of quartz until it melts. Quartz is used as the crucible's material because of its inertness. At this stage, doping can be initiated with impurity atoms such as boron or phosphorus being added to the molten silicon. Fixed amounts of dopants can yield desired characteristics in the semiconductor formed as a result of this procedure."

Equinox- "The time or date (twice each year) at which the sun crosses the celestial equation, when day and night have equal length (about 22 September and 20 March)".